nature cell biology

# A genetic screen identifies an LKB1–MARK signalling axis controlling the Hippo–YAP pathway

Morvarid Mohseni[1,2,3], Jianlong Sun[1,2,3], Allison Lau[1,3], Stephen Curtis[1,3,4], Jeffrey Goldsmith[5], Victor L. Fox[6], Chongjuan Wei[7], Marsha Frazier[7], Owen Samson[8], Kwok-Kin Wong[9,10], Carla Kim[1,3,4] and Fernando D. Camargo[1,2,3,11]

**The Hippo–YAP pathway is an emerging signalling cascade involved in the regulation of stem cell activity and organ size. To identify components of this pathway, we performed an RNAi-based kinome screen in human cells. Our screen identified several kinases not previously associated with Hippo signalling that control multiple cellular processes. One of the hits, LKB1, is a common tumour suppressor whose mechanism of action is only partially understood. We demonstrate that LKB1 acts through its substrates of the microtubule affinity-regulating kinase family to regulate the localization of the polarity determinant Scribble and the activity of the core Hippo kinases. Our data also indicate that YAP is functionally important for the tumour suppressive effects of LKB1. Our results identify a signalling axis that links YAP activation with *LKB1* mutations, and have implications for the treatment of *LKB1*-mutant human malignancies. In addition, our findings provide insight into upstream signals of the Hippo–YAP signalling cascade.**

Our understanding of human disease has benefited greatly from the study of developmental pathways in model organisms. Characterization of signalling cascades such as Wnt, Hedgehog and Notch has particularly contributed to the understanding and treatment of cancer[1]. A more recently discovered signalling cascade is the Hippo pathway, originally described in *Drosophila*, and proposed to be a means by which organ size can be regulated. This pathway is highly conserved in mammals, where the mammalian *hpo* orthologues, MST1/2, phosphorylate the large tumour suppressor (LATS1/2) kinases, which in turn phosphorylate the transcriptional co-activator YAP, restricting its activity and stability[2–4]. In the absence of phosphorylation, YAP translocates to the nucleus where it binds to the TEA-domain transcription factors[5,6] (TEAD1–4).

Activation of YAP, or loss of upstream negative regulators leads to striking overgrowth and tumour phenotypes in epithelial tissues, in many cases driven by the expansion of tissue-resident stem cells[3,4]. In addition, studies of human samples have demonstrated widespread Hippo pathway inactivation and nuclear YAP localization in multiple epithelial malignancies[7–9]. However, genomic analyses of common epithelial cancers have not revealed a significant rate of mutations in the known components of the pathway[10]. Recent data also suggest the presence of alternative kinases that might be responsible for YAP regulation[9,11]. Thus, common alterations of Hippo signalling in human cancer might be caused by mutations in genes not associated with the pathway at present.

Here, we have performed a genetic screen to identify kinases that impinge on the Hippo pathway. Our work uncovers kinases associated with multiple aspects of cellular function that are robust regulators of YAP localization and activity. These data provide important insight about the nature of inputs that speak to Hippo kinases. In addition, we identify the tumour suppressor LKB1 and its substrates of the microtubule affinity-regulating kinase (MARK) family as crucial regulators of the Hippo pathway. We present functional evidence suggesting that YAP is a critical component of the LKB1 tumour suppressive pathway. Our data have significant implications for the treatment of *Lkb1*-mutant cancers.

[1]Stem Cell Program, Boston Children's Hospital, Boston, Massachusetts 02115, USA. [2]Department of Stem Cell and Regenerative Biology, Harvard University, Cambridge, Massachusetts 02138, USA. [3]Harvard Stem Cell Institute, Cambridge, Massachusetts 02138, USA. [4]Department of Genetics, Harvard Medical School, Boston, Massachusetts 02115, USA. [5]Center for Pediatric Polyposis, Boston Children's Hospital, Boston, Massachusetts 02115, USA. [6]Division of Gastroenterology and Nutrition, Boston Children's Hospital, Boston, Massachusetts 02115, USA. [7]Department of Epidemiology, The University of Texas MD Anderson Cancer Center, Houston, Texas 77030, USA. [8]Wnt Signaling and Colorectal Cancer Group, The Beatson Institute for Cancer Research, Cancer Research UK, Glasgow G61 1BD, UK. [9]Genetics Division, Department of Medicine Brigham and Women's Hospital, Harvard Medical School, Boston, Massachusetts 02115, USA. [10]Ludwig Center at Dana-Farber/Harvard Cancer Center, Boston, Massachusetts 02115, USA.
[11]Correspondence should be addressed to F.D.C. (e-mail: Fernando.camargo@childrens.harvard.edu)

Received 13 May 2013; accepted 28 October 2013; published online 22 December 2013; corrected online 7 January 2014; DOI: 10.1038/ncb2884

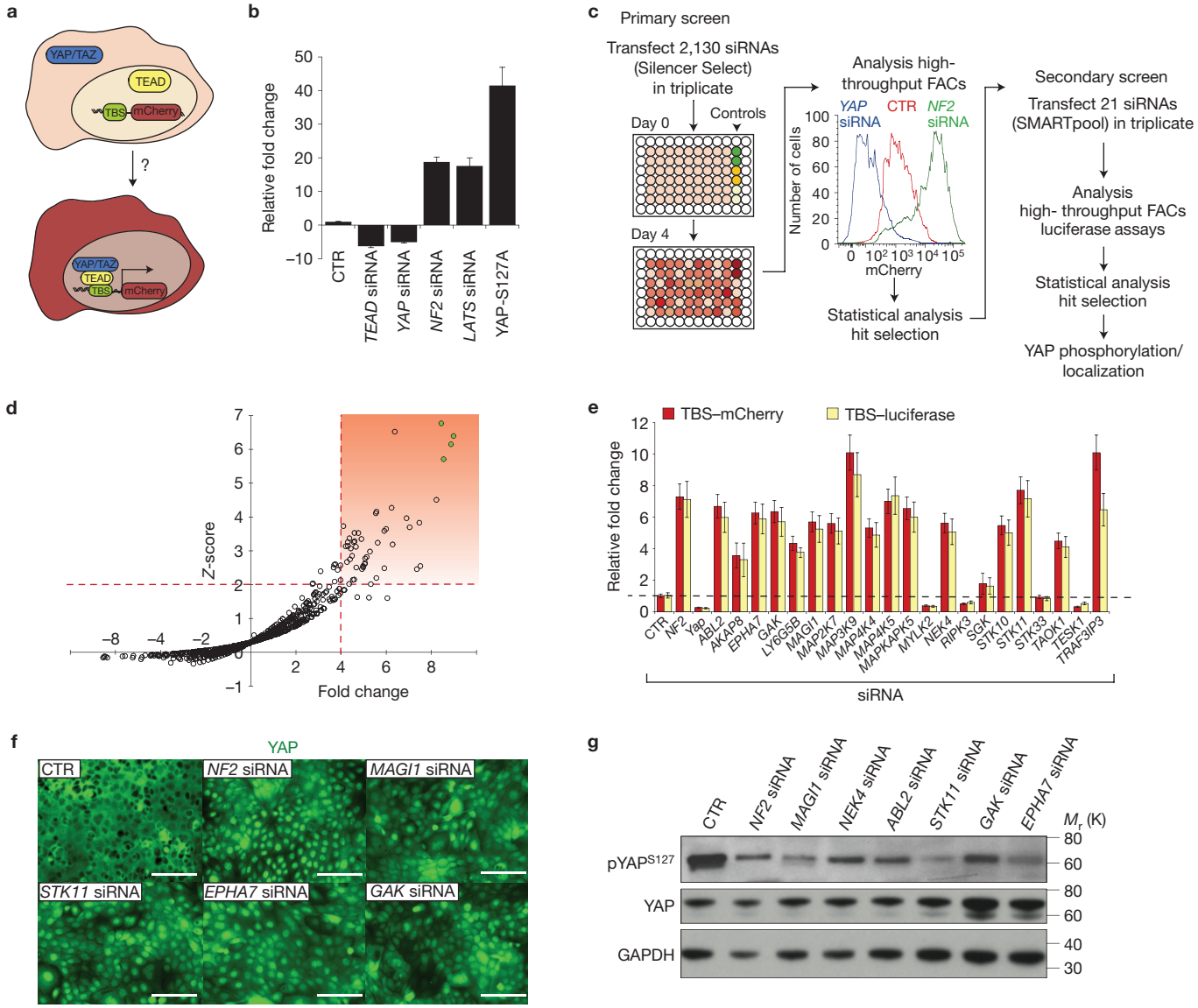


**Figure 1** A kinome RNAi screen identifies regulators of Hippo–YAP signalling. (**a**) Graphical representation of YAP-mediated STBS reporter activation in cells. (**b**) Validation of STBS reporter sensitivity using siRNA knockdown of known components of Hippo signalling. CTR, scrambled siRNA. $n = 5$ independent experiments. (**c**) Schematic of RNAi screening strategy. The RNAi screen was performed in 96-well plates using a stably expressing HEK293T STBS–mCherry reporter cell line. Activation of the STBS–mCherry reporter was visualized 4 days following siRNA transfection. Fluorescence intensity was captured by flow cytometry. Statistical analysis was performed to identify genes for secondary screening and final selection of hits. (**d**) Mean *Z*-score and mCherry reporter fold change (versus scrambled controls) values for each triplicate siRNA oligonucleotide were plotted to identify hits with statistical thresholds of *Z*-score >2 and fold change greater than 4. Highlighted rectangle represents hits satisfying these thresholds. Green filled circles represent siRNA knockdown of *LATS2* as a positive control. (**e**) A secondary siRNA screen identifies kinases that reproducibly raise STBS–mCherry reporter activity, performed using an alternative siRNA oligonucleotide source using two reporter systems. The secondary screen was repeated three times using pooled siRNAs. (**f**) YAP immunolocalization in HaCaT cells following siRNA knockdown of kinases that regulate STBS reporter activity. Representative images are shown; experiment repeated independently three times. Scale bars, 200 μm. (**g**) Immunoblot for Ser 127 YAP phosphorylation following siRNA knockdown of kinases from secondary screen. CTR represents scrambled siRNA and *NF2* siRNA is used as a positive control. Representative blots shown; experiment repeated three times. Also see uncropped figure scan in Supplementary figures. Error bars represent ± s.d. from $n = 3$ biological replicates.

## RESULTS

### A genetic screen identifies multiple Hippo-regulating kinases

To identify potential kinases that can repress YAP/TEAD activity, we developed an improved transcriptional reporter containing 14 copies of the known TEAD DNA-binding sequence (SuperTBS reporter; Fig. 1a)[11]. Functional assays revealed that this reporter faithfully recapitulated YAP/TEAD transcriptional activity, and was highly responsive to perturbations of endogenous upstream Hippo components such as LATS2 and the cytoskeleton-associated protein NF2 (refs 12,13 and Fig. 1b). Armed with a robust reporter for Hippo–YAP activity, we interrogated the effects of a human kinome short interfering RNA (siRNA) library containing 2,130 unique

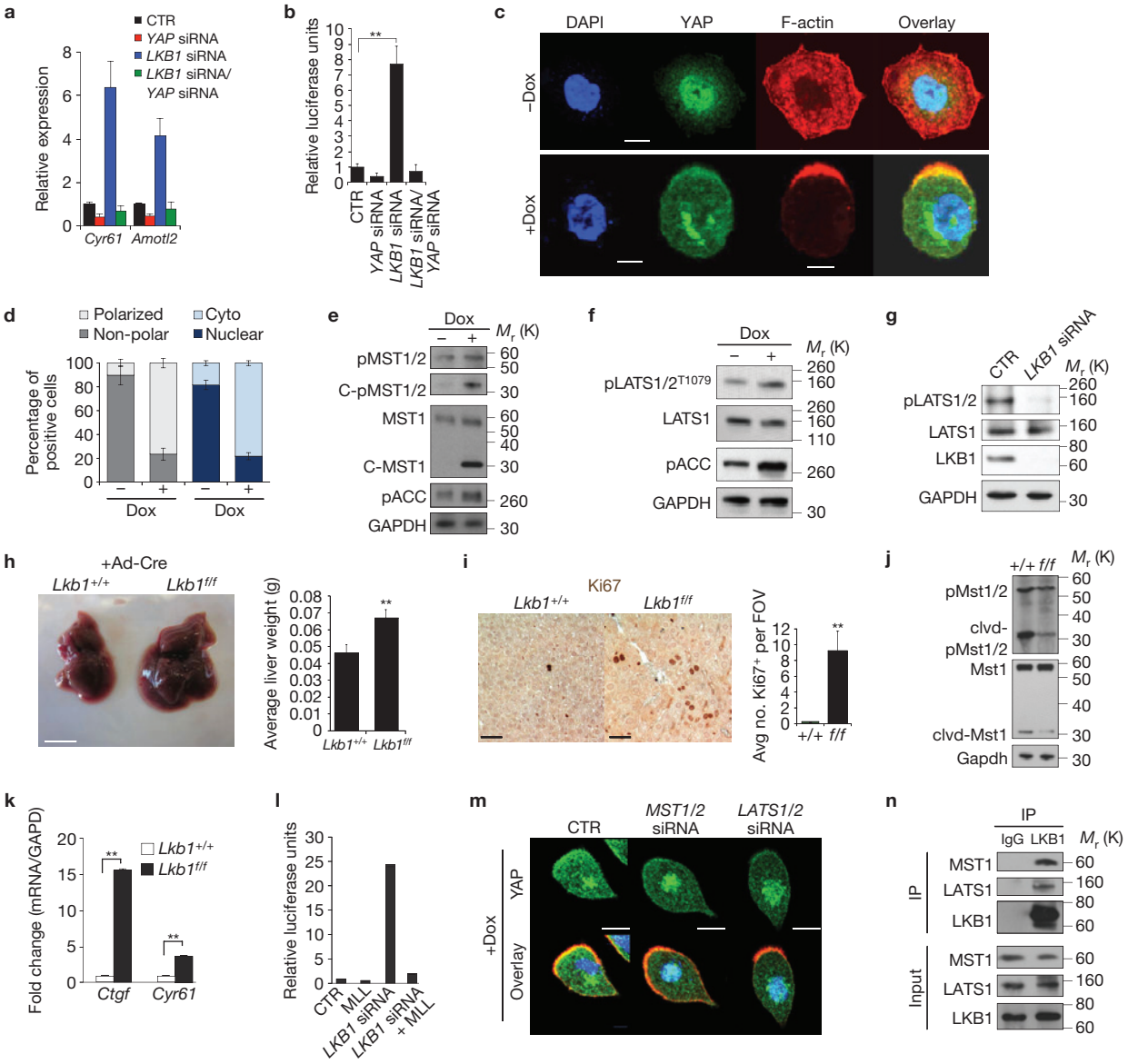


**Figure 2** LKB1 regulates YAP activity through the Hippo kinases. (**a**) *LKB1* knockdown induces YAP-dependent expression of target genes *Amotl2* and *Cyr61* (error bars represent mean ± s.d. from $n = 3$ biological replicates). (**b**) STBS–luciferase reporter (error bars represent mean ± s.d. from $n = 6$ biological replicates). (**c**) Immunofluorescence for F-actin (red), YAP (green) and nuclei (blue) in LS174T (W4) cells. Dox-inducible LKB1 activation after 24 h results in LKB1-dependent cell polarization and YAP nuclear to cytoplasmic translocation. Representative images shown; experiment repeated six times. Scale bars, 20 μm. (**d**) Quantification of cell polarization and YAP subcellular localization following Dox administration. Data are derived from three independent experiments where at least 300 cells were scored. Error bars represent mean ± s.d., $n = 3$. (**e**) MST1 activity in W4 cells is induced on LKB1 activation (+Dox). Note increased MST1/2 phosphorylation in the full-length and cleaved forms of MST1 and increase in levels of cleaved active MST1 peptide. Representative blots are shown; experiment repeated three times. Also see uncropped figure scan in Supplementary figures. (**f**) Activity of LATS1/2 is increased on LKB1 activation as measured by phosphorylation at Thr 1079 LATS1/2. Representative blots are shown; experiment repeated three times. (**g**) ATS1/2 phosphorylation at Thr 1079 is abolished on siRNA knockdown of LKB1 in MCF7 cells. (**h**) Ad-Cre-infected livers from *Lkb1* wild-type and *Lkb1*$^{f/f}$ mice exhibit an increase in liver size; error bars represent mean ± s.d. from $n = 6$ mice per group. Scale bar, 1 cm. (**i**) *Lkb1*-deficient murine livers exhibit an increase in cellular hepatocyte proliferation compared with *Lkb1* wild-type livers, $n = 6$ mice per group, 20 fields of view (FOV) counted for each sample in a group. Error bars represent mean ± s.d. (**j**) Western blot analysis performed on liver lysates derived from Ad-Cre-infected *Lkb1* $^{+/+}$ or *Lkb1*$^{f/f}$ mice 3 months post infection leads to an overall decrease in cleaved activated Mst1 and Thr 183/Thr 180 Mst1/2 phosphorylation and quantitative PCR of Yap target genes. See uncropped figure scan in Supplementary figures. Both lines of mice also carried a p53 homozygous floxed allele. (**k**) *Lkb1* loss *in vivo* also leads to an increase in YAP target expression. Data represent mean ± s.e.m., $n = 6$ mice treated with Ad-Cre. Experiment was repeated in two additional mice with similar results. (**l**) Overexpression of LATS1, LATS2 and MOB1 (MLL) in *LKB1*-knockdown HEK293T cells can restore STBS reporter activity. $n = 3$ independent experiments. (**m**) Knockdown of *MST1/2* and *LATS1/2* in Dox-treated W4 cells suppresses LKB1-driven cytoplasmic translocation of YAP (green) when compared with the scrambled negative control (CTR siRNA). Scale bars, 20 μm. (**n**) Endogenous co-immunoprecipitation experiments using HEK293T cells demonstrate physical association of LKB1 with LATS1 and MST1. Immunoblots represent one of three experiments performed. Also see uncropped figure scan in Supplementary figures. $^{**}P \leq 0.01$, two-tailed *t*-test.

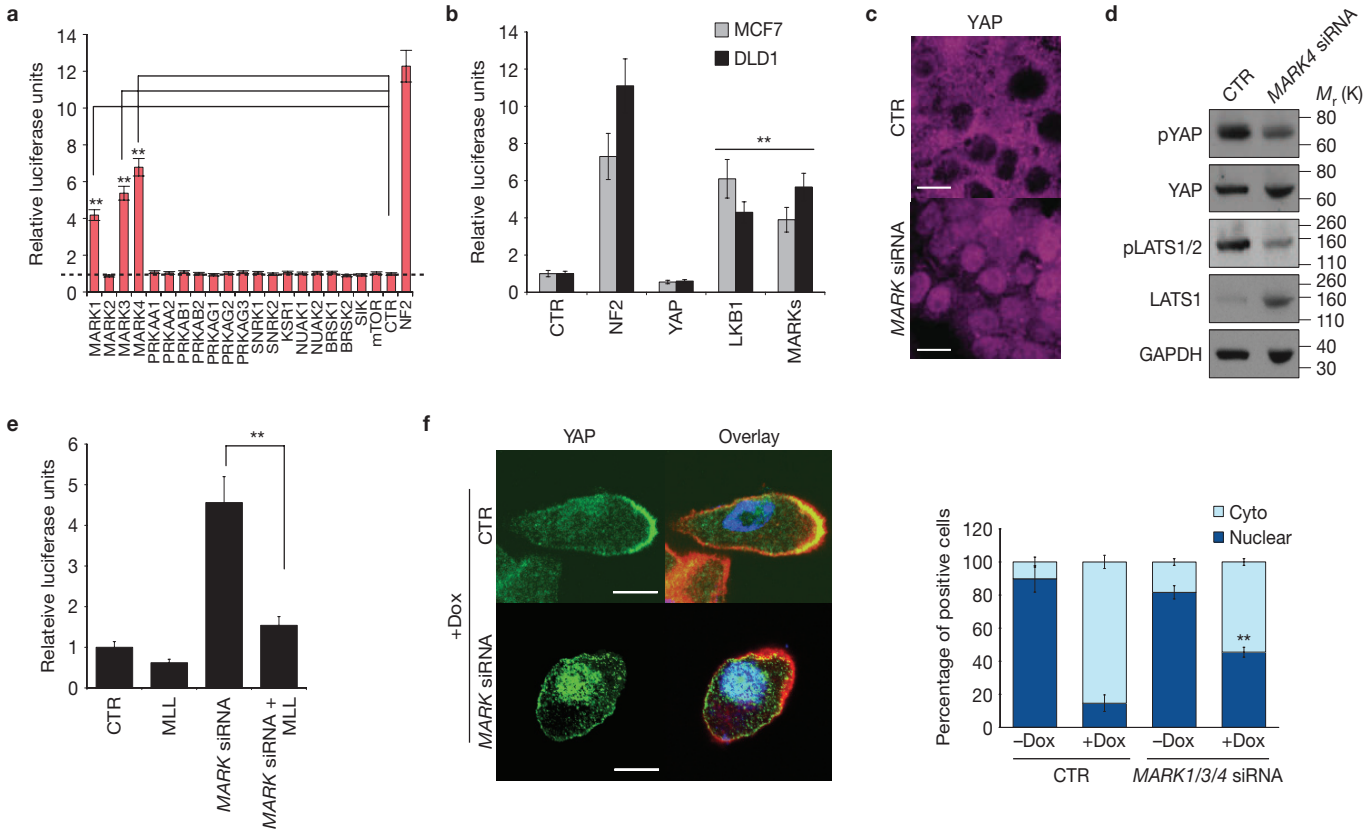


**Figure 3** MARKs act downstream of LKB1 to regulate Hippo–YAP. (**a**) Small-scale RNAi screen on downstream substrates of LKB1 in HEK293T STBS–Luc cells. Error bars represent ± standard deviation (s.d.) from $n = 3$ independent experiments. (**b**) Knockdown of MARKs (MARK1, 3 and 4) in MCF7 and DLD1 cells activates STBS–Luc. $n = 3$ individual experiments per group ± s.d. (**c**,**d**) Nuclear YAP accumulation (**c**) and decreases in LATS and YAP phosphorylation following knockdown of MARKs (**d**). (**e**) Repression of MARK-dependent STBS–Luc activity by overexpression of MOB1/LATS1/LATS2 (MLL). $n = 3$ biological replicates ± s.d. (**f**) Suppression of LKB1-driven cytoplasmic translocation of YAP following *MARK4* knockdown in Dox-treated W4 cells. Representative immunofluorescence images from three independent experiments. Right panel, quantification of the number of polarized cells in Dox-treated cells. *P* values calculated by comparing wild-type Dox-treated cells with those treated with *MARK* siRNA. Data are derived from four independent experiments where at least 300 cells were scored. Error bars represent mean ± s.d. from $n = 4$, $^{**}, P \leq 10.01$, two-tailed *t*-test. Scale bars, 20 μm.

siRNA oligonucleotides for 710 kinase genes in a HEK293T cell line stably carrying the reporter (Fig. 1c). Initial hits were identified by a statistical *Z*-score cutoff of 2 in addition to a >4-fold change of mean fluorescence intensity compared with scrambled siRNA controls (Fig. 1d). Our high-stringency statistical analysis revealed 21 kinases whose silencing resulted in enhanced STBS reporter activity (Fig. 1d and Supplementary Table 1). Through a secondary screen using a different commercial source of siRNAs to control for off-target effects, we confirmed that knockdown of 16 of these kinases robustly induced STBS reporter activity (Fig. 1e). Loss of 13 of these kinases also led to YAP nuclear accumulation even in high-density conditions where Hippo signalling is typically activated (Fig. 1f and Supplementary Fig. 1a). To further characterize these hits, we evaluated their effects on YAP phosphorylation at Ser 127, as this is a highly conserved direct-substrate site for LATS1/2 and is one of the best characterized biochemical markers for Hippo-mediated YAP inactivation[14]. Silencing of 8 of the 16 kinases resulted in decreases in $YAP^{S127}$ phosphorylation (Fig. 1g and Supplementary Fig. 1b), indicating that some of these molecules regulate YAP activity independently of Hippo.

Interestingly, four of the validated kinase hits (MAP2K7, MAP3K9, MAP4K4, MAP4K5) are part of an activating network of the c-Jun amino-terminal kinase (JNK) branch of the mitogen-activated kinase (MAP) pathway, a stress-activated cascade implicated in compensatory growth and tumorigenesis[15]. Silencing of these kinases does not lead to a reduction in YAP Ser 127 phosphorylation, indicating an alternative mode of YAP regulation (Supplementary Fig. 1b). A targeted analysis using RNA-interference (RNAi) and small-molecule manipulation confirmed that only the JNK arm of the MAP kinase pathway controlled YAP/TEAD reporter activity (Supplementary Fig. 1c,d). Although the role of JNK signalling in cancer is complex, our data support emerging findings suggesting that JNK activators are tumour suppressors, and implicate Hippo–YAP signalling as a downstream mechanism[16,17]. The ephrin receptor EPHA7 (Fig. 1d–g), implicated in providing cell-positioning cues during development and mutated in lung cancer and lymphomas[18,19], also regulates YAP activity. Intriguingly, other ephrin-type A receptors (EPHA4, EPHA5 and EPHA8; Supplementary Table 2) are also found to enhance STBS activity, indicating an important crosstalk between ephrin signalling and Hippo. We also identify MAGI1 (Fig. 1e–g and Supplementary Table 1), a growth

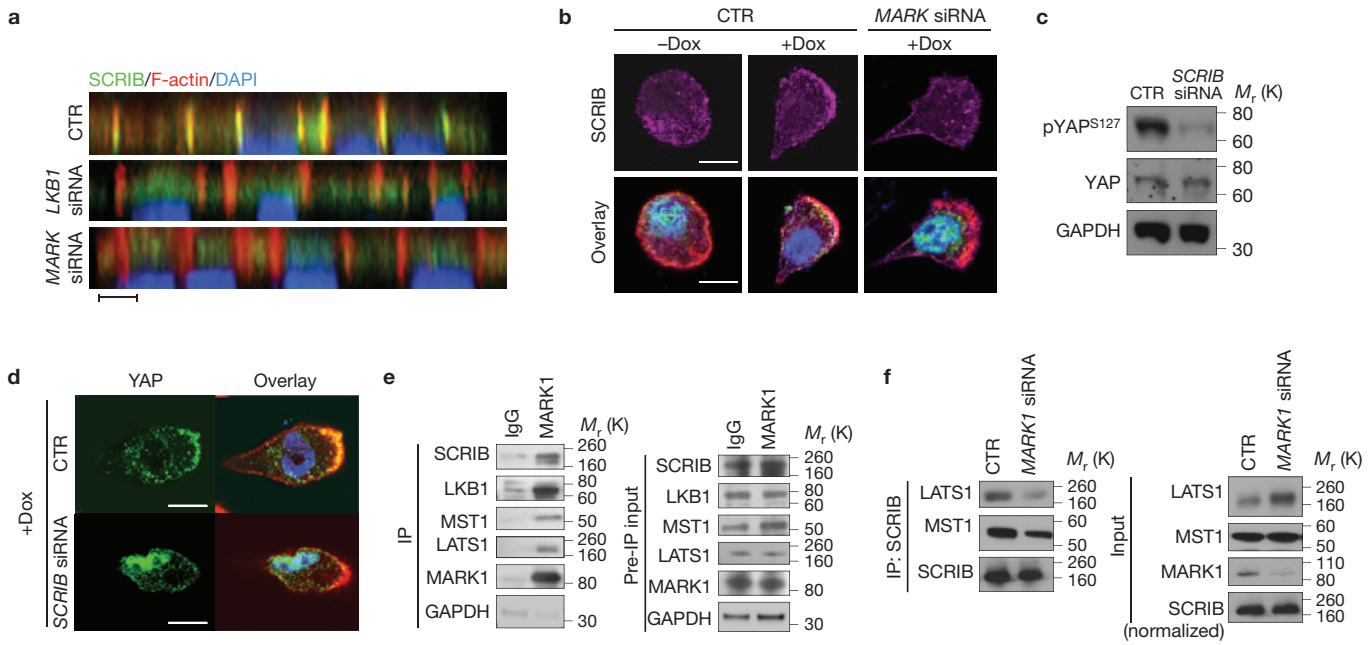


**Figure 4** Scribble acts downstream of LKB1 to regulate Hippo–YAP. (**a**) Confocal immunofluorescent and *Z*-stack analysis for Scribble (SCRIB, green), F-actin (red) and nuclei (blue) in LKB1 and MARK knockdown in MCF7 cells. Note mislocalization of SCRIB following *LKB1* or *MARK* silencing. Representative images from 4 independent experiments. (**b**) Immunofluorescence in W4 cells demonstrates that LKB1 activation leads to SCRIB re-localization to the cell membrane and actin cap and that this requires MARKs activity. (**c**) Knockdown of *SCRIB* in HEK293T cells reduces Ser 127 YAP phosphorylation. (**d**) Knockdown of *SCRIB* in Dox-induced LKB1-activated W4 cells suppressed YAP re-localization to the cytoplasm and actin cap. (**e**) Endogenous co-immunoprecipitation of MARK1 demonstrates potential interactions with LKB1, SCRIB, MST1 and LATS1. (**f**) The physical interaction between SCRIB and MST is reduced in the absence of MARK1. Adjusted lysate amounts were used to obtain equal levels of immunoprecipitated SCRIB. See uncropped figure scan in Supplementary Figures. Representative blots from at least 3 repeated experiments. Scale bars, 20 μm.

suppressive kinase also mutated in multiple human cancers[10,20]. GAK, a protein involved in clathrin-mediated endocytosis is also a hit[21], as are the microtubule regulating kinases NEK4 and TESK1 (ref. 22). Among the other regulators, a recently described Hippo-regulating kinase, TAOK1, was also identified (Fig. 1 and Supplementary Fig. 1a,b and Table 1 and ref. 23).

## LKB1 regulates YAP through MST/LATS

We were particularly interested by the fact that YAP phosphorylation was significantly repressed by STK11 knockdown (Fig. 1e–g). STK11, also known as LKB1, is a well-established human tumour suppressor that controls, among other things, cellular metabolism, proliferation and polarity[24]. The effect of LKB1 knockdown on YAP phosphorylation and localization was reproduced with multiple oligonucleotides and cell lines (Supplementary Fig. 2a–d). LKB1 knockdown also resulted in the upregulation of known YAP target genes, such as *Amotl2* and *Cyr61* (ref. 6 and Fig. 2a). This transcriptional response was entirely YAP-dependent, as endogenous target gene and reporter responses were suppressed in YAP/LKB1 double-knockdown cells (Fig. 2a,b and Supplementary Fig. 2e). To further demonstrate a regulatory role of LKB1 upstream of YAP we used an engineered intestinal epithelial cell line (W4) in which LKB1 activity could be induced following treatment with doxycycline[25] (Dox). Dox-dependent LKB1-activity is evidenced by polarization and actin cytoskeleton rearrangements (Fig. 2c,d). Whereas YAP is predominantly nuclear at low cell densities, stimulation of LKB1 activity induced a striking and significant shift of YAP localization into the cytoplasm and actin cap of polarized cells (Fig. 2c,d). Consistent with this, we observed a significant reduction of YAP/TEAD transcriptional activity in Dox-treated cells (Supplementary Fig. 2f). Our results are consistent with a recent report indicating YAP activation in LKB1-mutant cell lines[26].

We next determined whether LKB1 acts through the canonical Hippo kinases to regulate YAP. We observed increased MST1 activity, as measured by phosphorylation and the presence of a cleaved MST1 catalytic fragment following LKB1 activation in W4 cells (Fig. 2e). Similarly, LKB1 activation led to a marked increase in phosphorylation of Thr 1079 in LATS1/2 (Fig. 2f). This residue marks LATS1/2 activation by MST1/2 and its co-activator SAV1 (ref. 14). Correspondingly, LKB1 silencing led to loss of LATS1/2 Thr 1079 phosphorylation (Fig. 2g). To confirm that LKB1 is important for MST1/2 activation, we used a mouse model in which *Lkb1* was deleted in the liver using Ad-Cre. In agreement with MST1/2 loss-of-function phenotypes[9], *Lkb1* deletion resulted in hepatomegaly and increased hepatocyte proliferation (Supplementary Fig. 2g). As predicted, we also observed a significant decrease in the amount of cleaved and phosphorylated MST1 peptide in *Lkb1*-deficient livers (Fig. 2h and Supplementary Fig. 2h) and upregulation of YAP target genes (Fig. 2i). Supporting our findings that LKB1 acts upstream of the Hippo kinases, we find that expression of LATS1/2 and its co-activator MOB1 rescues the increase in YAP/TEAD transcriptional activity following knockdown of LKB1 (Fig. 2j). Furthermore, knockdown of MST1/2 or LATS1/2 in Dox-treated W4 cells significantly suppresses the LKB1-mediated shift in YAP subcellular localization

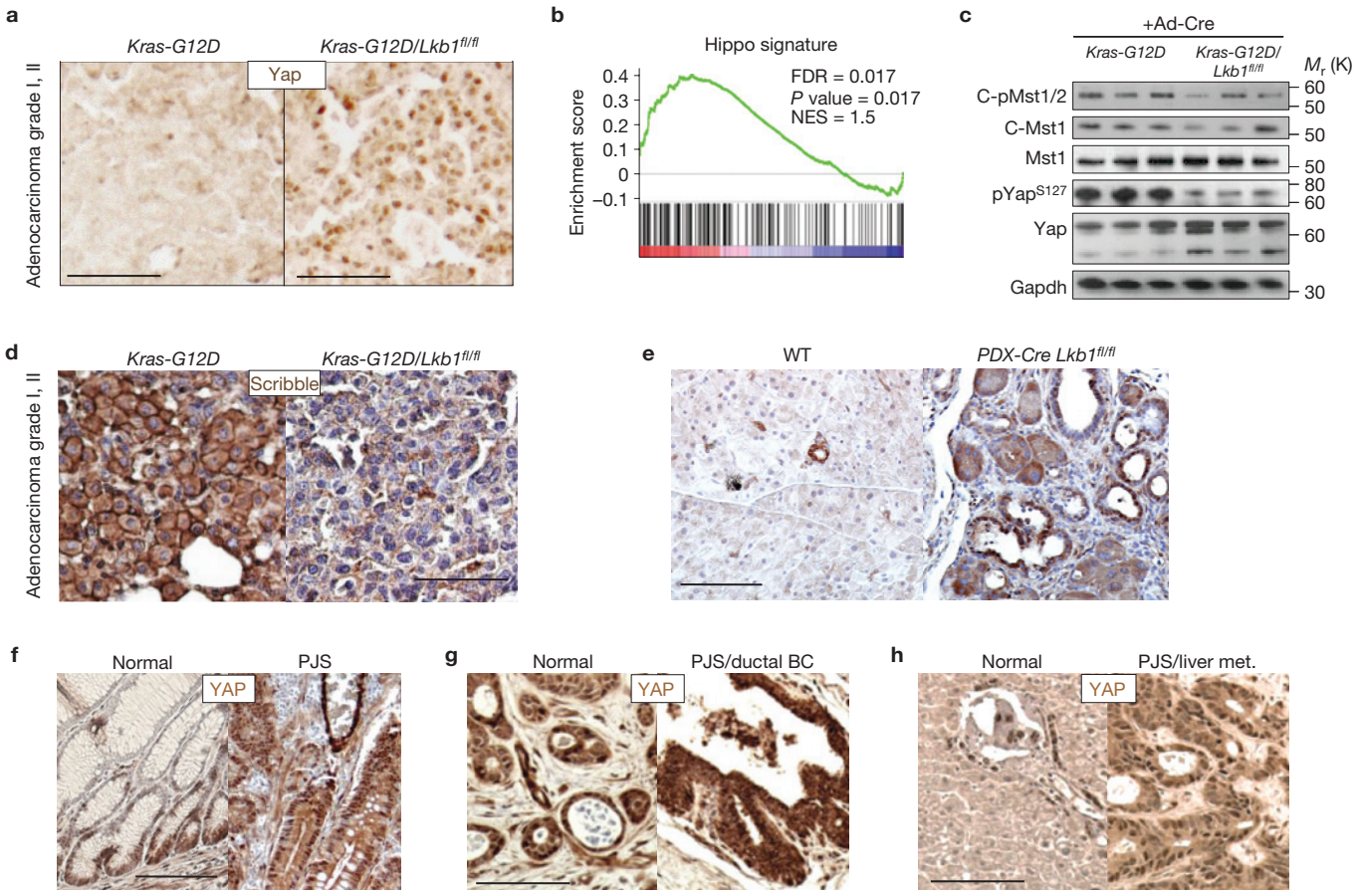


**Figure 5** Yap activity is enhanced in *Lkb1*-deficient tumours. (**a**) Immunohistochemistry for Yap on grade I–II lung adenocarcinomas derived from *Kras-G12D* mutant (K) and *Kras-G12D/Lkb1*$^{fl/fl}$ (KL) mice treated with intranasal Ad-Cre. Representative picture shown; $n = 5$ for each genotype. (**b**) Gene set enrichment analysis demonstrates significant enrichment of a transcriptional Hippo signature in KL versus K murine lung tumours. (**c**) Immunoblot analysis shows reduced active phosphorylated and cleaved forms of Mst1/2 in individual KL lung tumour nodules. Similarly, Ser 127 Yap phosphorylation is reduced ($n = 3$ mice). (**d**) Immunohistochemistry for Scribble localization in K and KL lung adenocarcinomas, ($n = 5$ mice). (**e**) Immunohistochemistry for Yap in pancreas from control pancreas (WT) or *Lkb1*-deficient tissue. (**f**) YAP localization assessed by immunohistochemistry in human intestinal tissue and PJS intestinal polyps. Representative data, $n = 3$ patients. (**g**) Immunohistochemistry for YAP localization and expression in normal ductal tissue compared with ductal breast adenocarcinoma (BC), and in normal human liver compared with metastatic liver adenocarcinoma derived from a PJS patient (**h**). Scale bars, 500 μm.

(Fig. 2k and Supplementary Fig. 2i–j). Supporting a regulatory role, we find that endogenous and overexpressed LKB1 can strongly interact with both LATS1 and MST1 in co-immunoprecipitation experiments (Fig. 2l and Supplementary Fig. 2k–l).

### LKB1 acts upstream of MARKs to regulate YAP

To shed light on a possible mechanism for regulation, we performed *in vitro* kinase assays and mass spectrometry analyses to determine whether MST1 or LATS2 could be direct targets of LKB1. Our results found no evidence for LKB1-mediated phosphorylation at potential consensus sites in either MST1 or LATS2, thus suggesting that the LKB1 effect on these kinases was indirect. We then performed a siRNA mini-screen evaluating most known downstream targets of LKB1 (ref. 27), including AMPK and mTOR, commonly implicated in growth suppression by LKB1, for their ability to regulate the STBS reporter. This screen revealed that three members of the MARK family (MARK1, 3 and 4; hereafter referred to as MARKs) were able to modulate TEAD-reporter activity (Fig. 3a). These kinases are also hits in our primary kinome screen if lower hit thresholds are selected (Supplementary Table 2). The effect of MARK knockdown was reproduced across several cell types and with multiple oligonucleotides (Fig. 3b and Supplementary Fig. 3a), and its effect on TEAD-reporter activity was also suppressed with concomitant knockdown of YAP (Supplementary Fig. 3b). Loss of MARK4 also results in enhanced YAP nuclear localization (Fig. 3c), and a decrease in LATS and YAP phosphorylation (Fig. 3d). Suggesting that MARKs also act upstream of the Hippo kinases, overexpression of LATS and MOB1 can fully suppress the MARK4 knockdown effect on TEAD-reporter activity (Fig. 3e and Supplementary Fig. 3c). To ascertain whether MARKs were functionally downstream of LKB1, we knocked down MARKs in LKB1-induced W4 cells. Dox addition to W4 cells leads to MARK1 activation[27] (Supplementary Fig. 3d), and silencing of MARKs in this context resulted in a significant loss of cytoplasmic YAP translocation (Fig. 3f and Supplementary Fig. 3e–f). Combined, these data demonstrate that LKB1 is exerting its effects on the Hippo pathway through its direct substrate, the MARKs.

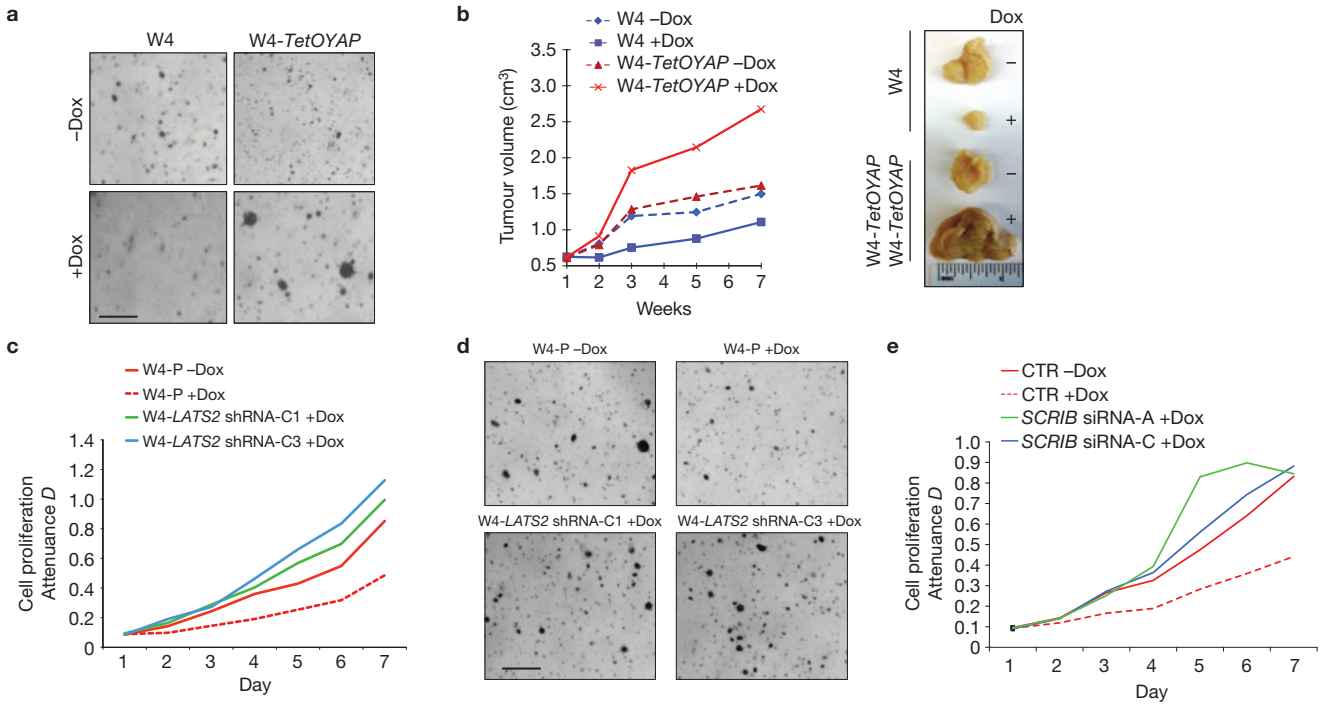


**Figure 6** YAP activation can overcome LKB1-driven tumour suppression. (**a**) Soft-agar colony-formation assay using W4 and W4 cells also expressing a Dox-inducible *YAP-S127A* transgene (*TetOYAP*). Shown are representative images of plates ± Dox 4 weeks after seeding. Experiment was repeated three times. (**b**) Subcutaneous xenograft assay using W4 and W4-*TetOYAP* cells. Tumour volumes for non-induced and induced tumours are shown. Representative tumours from non-induced and induced W4 and W4-*TetOYAP* xenografts are shown on the right. $n = 7$ mice per group (**c**) Proliferation assay for parental or W4 cells expressing either of two independent shRNAs against LATS2. Data are representative of three independent experiments performed. (**d**) Four-week soft-agar colony-formation assays of cells shown in **c**. (**e**) Proliferation assay for W4 cells that were also transfected with either of two siRNAs targeting SCRIB. Data are representative of three independent experiments performed. Scale bars, 200 μm.

### MARKs regulate SCRIB localization and Hippo kinase activity

MARKs are also known as the PAR-1 family of proteins and have been implicated in the regulation of cell polarity and microtubule dynamics through different mechanisms[28]. In *Drosophila*, the PAR-1 orthologue has been shown to phosphorylate and regulate localization of Discs large[29] (DLG), a member of the basolateral polarity complex also consisting of Lethal giant larvae (LGL) and Scribble[30,31] (SCRIB). Proper localization of SCRIB is required for Hippo pathway activity in both *Drosophila* and mammalian cells[32–34]. Thus, we posited that LKB1 could be regulating Hippo–YAP activity through regulation of the basolateral polarity complex by the MARKs. Indeed, we find that MARKs knockdown results in mislocalization of SCRIB (Fig. 4a and Supplementary Fig. 4a), and reduction of SCRIB protein (Supplementary Fig. 4b–c). Demonstrating a direct role for LKB1 and MARKs in the localization of SCRIB, Dox-mediated activation of LKB1 in W4 cells results in SCRIB recruitment to the cellular membrane and the actin cap (Fig. 4b). Knockdown of MARKs in this context reduces the sub-cellular localization shift of SCRIB (Fig. 4b). As predicted, SCRIB knockdown also leads to an increase in TEAD-reporter activity and a decrease in YAP phosphorylation (Fig. 4c and Supplementary Fig. 4e). Importantly, knockdown of SCRIB in LKB1-activated W4 cells significantly rescues the shift of YAP localization to the cytoplasm and actin cap (Fig. 4d and Supplementary Fig. 4f–h), indicating that SCRIB is critical for LKB1-mediated regulation of YAP. Moreover, co-immunoprecipitation experiments demonstrate that endogenous MARK1 or overexpressed MARK4 can be detected in a complex with LKB1, MST1, LATS1 and SCRIB (Fig. 4e and Supplementary Fig. 4i), indicating the existence of a Hippo regulatory protein complex. It has been proposed that association of SCRIB with MST1/2 is important for the activation of the Hippo cascade[34]. We find that this association is highly dependent on MARKs (Fig. 4f and Supplementary Fig. 4j), as their loss impairs the interaction of both MST1/2 and LATS1/2 with SCRIB.

### YAP activation is a hallmark of LKB1-mutant tumours

*Lkb1* germline mutations are associated with Peutz–Jeghers syndrome (PJS), an inherited disorder in which patients develop intestinal polyps and are at higher risk for developing multiple malignancies[35]. *Lkb1* alterations are also present in many types of sporadic epithelial cancer, particularly lung and pancreatic carcinomas[35]. Loss of Lkb1 in mice is associated with more aggressive and metastatic potential of lung tumours[36]. To corroborate our *in vitro* observations, we evaluated the status of Hippo signalling in lung tumours derived from mice carrying an activating *K-Ras* mutation (K) or the K-*Ras* transgene and concomitant *Lkb1* deletion (KL). Strikingly, we find that stage-matched KL adenocarcinomas were strongly positive for nuclear YAP in contrast to K tumours, which exhibit predominantly cytoplasmic and diffuse YAP localization (Fig. 5a). To further assess the extent of YAP transcriptional activity in *Lkb1*-null tumours, we carried out gene set enrichment analysis to examine the enrichment of a YAP transcriptional signature derived in our laboratory (Supplementary Fig. 5a). Gene set enrichment analysis demonstrates

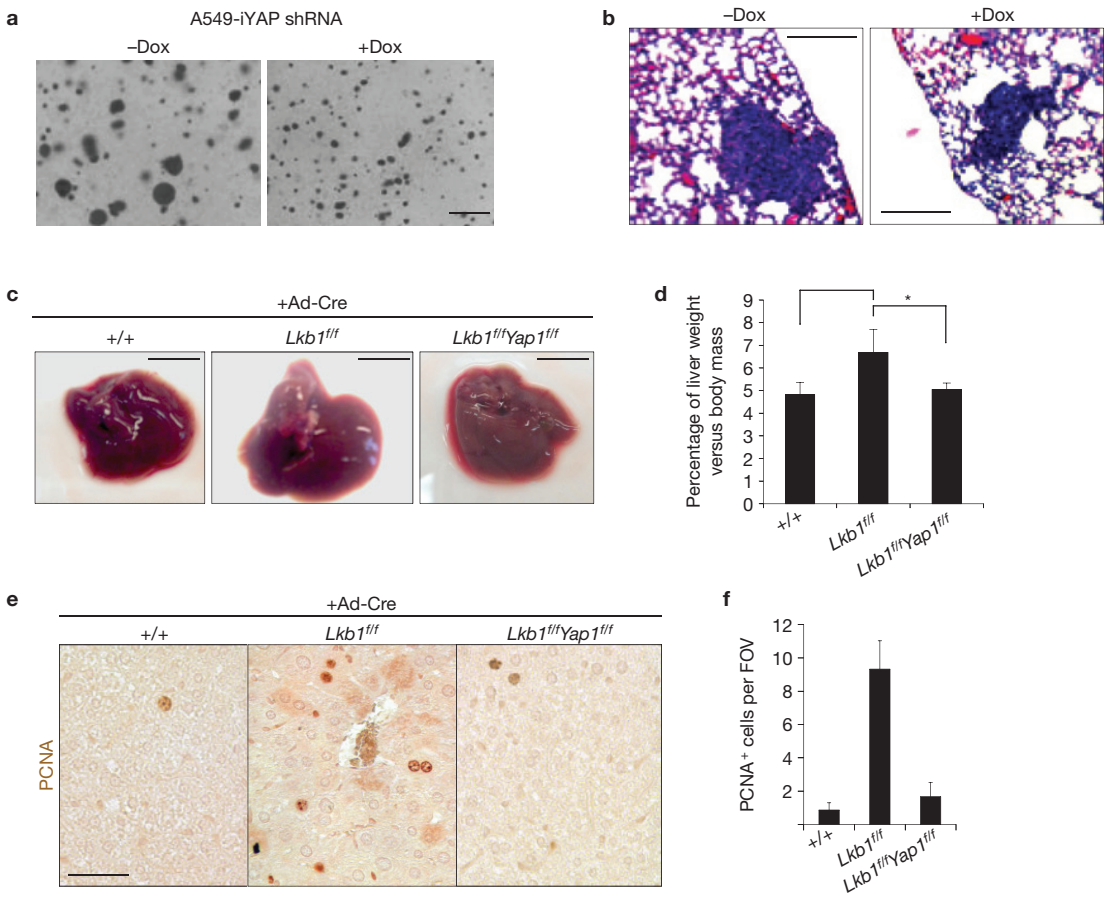


**Figure 7** YAP is essential for the growth of Lkb1-mutant tumours and tissue. (**a**) Four-week soft-agar assay using the *Lkb1*-deficient lung adenocarcinoma line A549. These cells expressed a Dox-inducible shRNA against YAP (iYAP shRNA). Scale bar 100 μm. (**b**) Representative images of metastatic lesions following intravenous injection of parental or iYAP shRNA A549 cells. Dox treatment of hosts was carried for 2 months at which time lung tissue was collected. Scale bars, 200 μm. (**c**,**d**) Ad-Cre-mediated deletion of a conditional allele of *Yap1* following Ad-Cre intravenous administration leads to significant suppression of hepatomegaly and hepatocyte hyperplasia. Scale bar, 1 cm. Animals received Ad-Cre at 1 month of age and tissues were collected 2.5 months later. (**e**) PCNA immunohistochemistry on Ad-Cre-treated mouse livers from wild-type, *Lkb1* and *Lkb1/Yap1* mutant mice. Scale bars, 500 μm. $n = 5$ mice per genotype. (**f**) Quantification of the average number of PCNA-positive cells per field of view from **e**. $n = 5$ mice per genotype, 20 fields of view. Error bars represent ± s.d. from $n = 5$ mice. $^{*}P \leq 0.05$, two-tailed $t$-test.

a highly significant enrichment of this YAP signature in KL tumours (Fig. 5b). Furthermore, biochemical analyses of tumour nodules also demonstrate decreased MST1/2 and YAP Ser 127 phosphorylation in the KL genotype (Fig. 5c). Furthermore, as predicted from our model, SCRIB localization is markedly altered and its expression reduced in KL tumours (Fig. 5d). We also evaluated YAP status in a model of pancreatic neoplasia derived from tissue-specific deletion of *Lkb1*. Consistent with the lung tumour data, *Lkb1*-null pancreatic ductal adenocarcinomas exhibit robust YAP nuclear localization compared with control tissue (Fig. 5e).

Moreover, we find that gastrointestinal polyps of human PJS patients exhibit an increase in nuclear YAP localization in both epithelial and smooth muscle cells compared with normal colon or juvenile polyposis polyps carrying *SMAD4* mutations (Fig. 5f and Supplementary Fig. 5b). Examination of a malignant ductal breast adenocarcinoma and metastatic liver disease that developed in a PJS patient further revealed strong YAP nuclear accumulation in the tumour (Fig. 5g,h). Taken together, these data show that genetic deletion of *Lkb1* in both murine and human tissue leads to enhanced nuclear YAP activity.

## YAP is functionally important downstream of LKB1

We next investigated functionally whether YAP acted downstream of LKB1 in tumour suppression. Using W4 cells, we found that inducible LKB1 activation has a powerful growth suppressive function *in vitro* (Fig. 6a and Supplementary Fig. 6a), and in xenografts (Fig. 6b and Supplementary Fig. 6b). However, expression of a YAP-S217A mutant protein is able to significantly overcome all of LKB1 tumour suppressive effects (Fig. 6a,b and Supplementary Fig. 6a,b). Silencing of either LATS2 or SCRIB also rescues growth suppression by LKB1 activation (Fig. 6d–f and Supplementary Fig. 6c,d). To determine whether we could reverse the effects of *LKB1* loss by manipulating YAP-expression levels, we developed a Dox-inducible YAP short hairpin RNA (shRNA) A549 cell line (Supplementary Fig. 7a). A549 is a lung cancer cell line mutant for *LKB1* widely used in tumour growth and metastasis assays[36]. In both a soft-agar colony-formation assay, and *in vivo* metastatic assays, we find that YAP depletion following Dox-treatment reduces the number and/or size of colonies and tumours (Fig. 7a,b and Supplementary Fig. 7a–c). Lung adenocarcinoma cell lines that are wild type for *LKB1* and expressed lower levels of YAP were

insensitive to YAP modulation (Supplementary Fig. 7d–f). Finally, we used Ad-Cre infection in mice to demonstrate that conditional deletion of *Yap1* suppresses the liver overgrowth phenotype (Fig. 7c,d) and hepatocyte hyperplasia observed following acute deletion of *Lkb1* (Fig. 7e,f and Supplementary Fig. 7g). Together these data provide multiple lines of evidence that Hippo–YAP is a functionally critical pathway downstream of LKB1.

## DISCUSSION

One important question in the Hippo–YAP field relates to the upstream signals that regulate the Hippo kinases. Our studies here have identified many molecules and pathways that might impinge on Hippo activity and growth control. As many of these kinases are also mutated in human cancer, their identification as regulators of YAP might provide a molecular explanation for the observations that YAP is highly active in numerous epithelial tumours, where mutations in the canonical Hippo components are not found.

The tumour suppressive function of LKB1 has primarily been linked to its ability to regulate cellular metabolism through AMPK activation[37]. LKB1 is linked to mTOR through the sequential activation of AMPK and the tumour suppressor TSC2, whose activation leads to suppression of mTOR activity[38]. It has been shown that polyps from PJS patients show upregulated mTOR activity, as do pancreata, cardiomyocytes and endometria of *Lkb1*-deficient mice. Treatment of endometrial LKB1-mutant adenocarcinomas with rapamycin and mTOR inhibitor, leads to regression of these tumours, supporting a functional role for mTOR downstream of LKb1 (ref. 38). Our studies here suggest that LKB1 can also exert its tumour suppressive effects through activation of a PAR-1-mediated polarity axis that controls the Hippo signalling pathway. Our data demonstrating that YAP loss could completely rescue growth phenotypes mediated by LKB1 loss *in vivo* suggest that this might a central mechanism. On this note, it has been shown that YAP can lead to mTOR activity through transcriptional activation of miR-29. Thus, YAP activation due to LKB1 alterations could also lead to mTORC1 activation.

Our data provide insight into a signalling axis downstream of LKB1 and PAR-1 kinases that regulates the interaction of the Hippo kinases with SCRIB and perhaps other components of the basolateral polarity complex. MARKs can also lead to changes in polarity by antagonizing the PAR-3/PAR-6 polarity complex[39]. This complex is localized apically whereas PAR-3 lacking PAR-1 phosphorylation results in ectopic lateral mislocalization. Under normal conditions, the lateral exclusion of PAR-3/PAR-6 by PAR-1 also cooperates with Crumbs to restrict Par-3 localization, and loss of both pathways disrupts epithelial polarity[39]. The literature supports that the Hippo pathway is indeed regulated by these polarity complexes[32,40]. Whether Par-3, Par-6, Crumbs and other substrates of Par-1/MARKs are also involved in controlling SCRIB remains to be investigated. Similarly, a connection between Hippo–YAP signalling and the actin cytoskeleton has recently been demonstrated[41]. Considering that LKB1 and SCRIB have effects on the actin cytoskeleton[42,43], it is possible that actin fibre regulation could be an additional mechanism by which LKB1 modulates YAP activity. LKB1 is then a candidate upstream regulator of the multiple inputs that impinge on YAP activity. Collectively, these data suggest that manipulation of the Hippo signalling pathway should now be evaluated for the treatment of LKB1 mutant cancers. □

## METHODS

Methods and any associated references are available in the online version of the paper.

*Note: Supplementary Information is available in the online version of the paper*

### ACKNOWLEDGEMENTS

We are grateful for stimulating and insightful discussions by members of the Camargo laboratory. Special thanks to R. Bronson of the Harvard Rodent Facility and R. Mathieu of the Stem Cell Program FACS facility. We are grateful to N. Bardeesy for *Lkb1* conditional mice. This study was supported by awards from Stand Up to Cancer-AACR initiative (F.D.C.), NIH grant R01 CA131426 (F.D.C.) and DOD 81XWH-10-1-0724. M.M. is a DOD-CDMRP Postdoctoral Fellow. F.D.C. is a Pew Scholar in the Biomedical Sciences.

### AUTHOR CONTRIBUTIONS

M.M. and F.D.C. designed the study and wrote the paper. M.M., J.S., A.L. and S.C. performed the experimental work. J.G., V.L.F., C.W. and M.F. provided human clinical tissue. O.S., K-K.W. and C.K. provided mouse tumour samples. C.K. and K-K.W. analysed the data.

### COMPETING FINANCIAL INTERESTS

The authors declare no competing financial interests.

Published online at www.nature.com/doifinder/10.1038/ncb2884
Reprints and permissions information is available online at www.nature.com/reprints

1. Takebe, N., Harris, P. J., Warren, R. Q. & Ivy, S. P. Targeting cancer stem cells by inhibiting Wnt, Notch, and Hedgehog pathways. *Nat. Rev. Clin. Oncol.* **8,** 97–106 (2011).
2. Zhao, B., Lei, Q. Y. & Guan, K. L. The Hippo-YAP pathway: new connections between regulation of organ size and cancer. *Curr. Opin. Cell Biol.* **20,** 638–646 (2008).
3. Ramos, A. & Camargo, F. D. The Hippo signaling pathway and stem cell biology. *Trends Cell Biol.* **22,** 339–346 (2012).
4. Pan, D. The hippo signaling pathway in development and cancer. *Dev. Cell* **19,** 491–505 (2010).
5. Ota, M. & Sasaki, H. Mammalian Tead proteins regulate cell proliferation and contact inhibition as transcriptional mediators of Hippo signaling. *Development* **135,** 4059–4069 (2008).
6. Zhao, B. *et al.* TEAD mediates YAP-dependent gene induction and growth control. *Genes Dev.* **22,** 1962–1971 (2008).
7. Steinhardt, A. A. *et al.* Expression of Yes-associated protein in common solid tumors. *Human Pathol.* **39,** 1582–1589 (2008).
8. Zhang, X. *et al.* The Hippo pathway transcriptional co-activator, YAP, is an ovarian cancer oncogene. *Oncogene* **30,** 2810–2822 (2011).
9. Zhou, D. *et al.* Mst1 and Mst2 maintain hepatocyte quiescence and suppress hepatocellular carcinoma development through inactivation of the YAP oncogene. *Cancer Cell* **16,** 425–438 (2009).
10. Bamford, S. *et al.* The COSMIC (Catalogue of Somatic Mutations in Cancer) database and website. *Br. J. Cancer* **19,** 355–358 (2004).
11. Schlegelmilch, K. *et al.* YAP acts downstream of alpha-catenin to control epidermal proliferation. *Cell* **144,** 782–795 (2011).
12. Zhang, N. *et al.* The Merlin/NF2 tumor suppressor functions through the YAP oncoprotein to regulate tissue homeostasis in mammals. *Dev. Cell* **19,** 27–38 (2010).
13. Hamaratoglu, F. *et al.* The tumour-suppressor genes NF2/Merlin and Expanded act through Hippo signalling to regulate cell proliferation and apoptosis. *Nat. Cell Biol.* **8,** 27–36 (2006).
14. Zhao, B. *et al.* Inactivation of YAP oncoprotein by the Hippo pathway is involved in cell contact inhibition and tissue growth control. *Genes Dev.* **21,** 2747–2761 (2007).
15. Chen, F. JNK-induced apoptosis, compensatory growth, and cancer stem cells. *Cancer Res.* **72,** 379–386 (2012).
16. Stark, M. S. *et al.* Frequent somatic mutations in MAP3K5 and MAP3K9 in metastatic melanoma identified by exome sequencing. *Nat. Genet.* **44,** 165–169 (2012).
17. Schramek, D. *et al.* The stress kinase MKK7 couples oncogenic stress to p53 stability and tumor suppression. *Nat. Genet.* **43,** 212–219 (2011).
18. Peifer, M. *et al.* Integrative genome analyses identify key somatic driver mutations of small-cell lung cancer. *Nat. Genet.* **44,** 1104–1110 (2012).
19. Oricchio, E. *et al.* The Eph-receptor A7 is a soluble tumor suppressor for follicular lymphoma. *Cell* **147,** 554–564 (2011).

20. Zaric, J. *et al*. Identification of MAGI1 as a tumor-suppressor protein induced by cyclooxygenase-2 inhibitors in colorectal cancer cells. *Oncogene* **31,** 48–59 (2012).
21. Lee, D. W., Zhao, X., Yim, Y. I., Eisenberg, E. & Greene, L. E. Essential role of cyclin-G-associated kinase (Auxilin-2) in developing and mature mice. *Mol. Biol. Cell* **19,** 2766–2776 (2008).
22. Doles, J. & Hemann, M. T. Nek4 status differentially alters sensitivity to distinct microtubule poisons. *Cancer Res.* **70,** 1033–1041 (2010).
23. Boggiano, J. C., Vanderzalm, P. J. & Fehon, R. G. Tao-1 phosphorylates Hippo/MST kinases to regulate the Hippo-Salvador-Warts tumor suppressor pathway. *Dev. Cell* **21,** 888–895 (2011).
24. Baas, A. F., Smit, L. & Clevers, H. LKB1 tumor suppressor protein: PARtaker in cell polarity. *Trends Cell Biol.* **14,** 312–319 (2004).
25. Baas, A.F. *et al*. Complete polarization of single intestinal epithelial cells upon activation of LKB1 by STRAD. *Cell* **116,** 457–466 (2004).
26. Nguyen, H. B., Babcock, J. T., Wells, C. D. & Quilliam, L. A. LKB1 tumor suppressor regulates AMP kinase/mTOR-independent cell growth and proliferation via the phosphorylation of YAP. *Oncogene* **32,** 4100–4109 (2013).
27. Lizcano, J. M. *et al*. LKB1 is a master kinase that activates 13 kinases of the AMPK subfamily, including MARK/PAR-1. *EMBO J.* **23,** 833–843 (2004).
28. Hurov, J. & Piwnica-Worms, H. The Par-1/MARK family of protein kinases: from polarity to metabolism. *Cell Cycle* **6,** 1966–1969 (2007).
29. Zhang, Y. *et al*. PAR-1 kinase phosphorylates Dlg and regulates its postsynaptic targeting at the Drosophila neuromuscular junction. *Neuron* **53,** 201–215 (2007).
30. Bilder, D., Li, M. & Perrimon, N. Cooperative regulation of cell polarity and growth by Drosophila tumor suppressors. *Science* **289,** 113–116 (2000).
31. Yamanaka, T. & Ohno, S. Role of Lgl/Dlg/Scribble in the regulation of epithelial junction, polarity and growth. *Front Biosci.* **13,** 6693–6707 (2008).
32. Grzeschik, N. A., Parsons, L. M., Allott, M. L., Harvey, K. F. & Richardson, H. E. Lgl, aPKC, and Crumbs regulate the Salvador/Warts/Hippo pathway through two distinct mechanisms. *Curr. Biol.* **20,** 573–581 (2010).
33. Parsons, L. M., Grzeschik, N. A., Allott, M. L. & Richardson, H. E. Lgl/aPKC and Crb regulate the Salvador/Warts/Hippo pathway. *Fly (Austin)* **4,** 288–293 (2010).
34. Cordenonsi, M. *et al*. The Hippo transducer TAZ confers cancer stem cell-related traits on breast cancer cells. *Cell* **147,** 759–772 (2011).
35. Sanchez-Cespedes, M. A role for LKB1 gene in human cancer beyond the Peutz-Jeghers syndrome. *Oncogene* **26,** 7825–7832 (2007).
36. Ji, H. *et al*. LKB1 modulates lung cancer differentiation and metastasis. *Nature* **448,** 807–810 (2007).
37. Katajisto, P. *et al*. The LKB1 tumor suppressor kinase in human disease. *Biochim. Biophys. Acta* **1775,** 63–75 (2007).
38. Zhou, W., Marcus, A. I. & Vertino, P. Dysregulation of mTOR activity through LKB1 inactivation. *Chin. J. Cancer* **32,** 427–433 (2013).
39. Benton, R. & St Johnston, D. Drosophila PAR-1 and 14-3-3 inhibit Bazooka/PAR-3 to establish complementary cortical domains in polarized cells. *Cell* **115,** 691–704 (2003).
40. Varelas, X. *et al*. The Crumbs complex couples cell density sensing to Hippo-dependent control of the TGF-beta-SMAD pathway. *Dev. Cell* **19,** 831–844 (2010).
41. Sansores-Garcia, L. *et al*. Modulating F-actin organization induces organ growth by affecting the Hippo pathway. *EMBO J.* **30,** 2325–2335 (2011).
42. Osmani, N., Vitale, N., Borg, J. P. & Etienne-Manneville, S. Scrib controls Cdc42 localization and activity to promote cell polarization during astrocyte migration. *Curr. Biol.* **16,** 2395–2405 (2006).
43. Xu, X., Omelchenko, T. & Hall, A. LKB1 tumor suppressor protein regulates actin filament assembly through Rho and its exchange factor Dbl independently of kinase activity. *BMC Cell Biol.* **11,** 77 (2010).

DOI: 10.1038/ncb2884

## METHODS

**RNAi screen.** An RNAi library against all known kinases in the human genome was used (Ambion *Silencer* Select Human Kinase siRNA Library, catalogue # 4397918). Reverse transfection using 0.1 µl of transfection reagent (RNAi max, Invitrogen) and siRNA of a final concentration of 5 nM was performed on approximately 10,000 HEK293T TBS–mCherry cells per well of a 96-well plate. We estimate that close to 98% of HEK293T cells are transfected using this method. The screen was performed in triplicate, with 3 oligonucleotides for each gene (Fig. 1d). To ensure limited edge effects, outer rows and columns were not used and instead were occupied by cell media. At 96 h post-transfection, HEK293T cells in negative control wells are confluent. Plates are subsequently trypsinized in 20 µl of trypsin/EDTA and inactivated in 30 µl of DMEM/10% FBS and analysed by flow cytometry using Texas red and GFP (HTS, BD LSRII) to obtain the mean fluorescent intensity of each cell. Data were collected and analysed using FACSDiva 6.0 (BD Biosciences). For follow-up work, individual oligonucleotides targeting YAP (s20366), LATS1 (s17392), LATS2 (s25503), MST1 (s13570), MST2 (s13567), SCRIB (s23970), MARK1 (#s8512), MARK4 (s33718) and NF2 (s194647), all from Ambion, were used.

**Hit selection.** Positive hits for each gene were identified as follows. $Z$-scores and fold changes were calculated for each oligonucleotide when compared with the negative control for each individual 96-well plate. Rigorous hit selection was performed by eliminating data that did not reproduce in at least two out of the three experiments for each oligonucleotide. Subsequently, these data were further filtered to identify oligonucleotides that reproducibly have a $Z$-score $> 2$ and fold change $> 4$. The final hit selection is based on the mean $Z$-score values and mean fold changes of each oligonucleotide for each gene, and if two or more oligonucleotides for each gene met these thresholds.

**Immunofluorescence.** Cells were seeded in a 24-well plate on sterilized glass coverslips overnight and then fixed in 4% paraformaldehyde/PBS for 10 min at room temperature, followed by three washes in PBS. Cells are permeabilized in 0.01% Triton/PBS for 1 min, followed by three washes in 0.01% Tween/PBS. Cells were then incubated in blocking buffer (0.5% FBS/PBS/0.01%Tween) for 1 h at room temperature and then incubated overnight at 4 °C in primary antibody (YAP 1:1,000, Cell Signaling #4912; Scribble 1:1,000, Santa Cruz #1049; GFP 1:500, Abcam #ab290) in blocking buffer. Coverslips were washed three times in 0.01%/PBS Tween and then incubated in secondary antibody and/or Alexa-fluor Phalloidin (1:5,000, Molecular Probes #A12381) for 1 h at room temperature. Coverslips were washed 3 times in 0.01%/PBS Tween and once in PBS before mounting on slides (ProLong Gold Antifade Reagent with DAPI, Life Technologies #P36935). Immunofluorescence imaging was performed using the Zeiss LSM 700 Laser Scanning Confocal with the following objectives: ×10 Zeiss EC plan-NEOFLUAR dry, 0.3 NA; ×25 Zeiss plan-NEOFLUAR multi-immersion, 0.75 NA; ×63 Zeiss plan-APOCHROMAT oil, 1.4 NA; ×100 Zeiss plan-APOCHROMAT oil, 1.3 NA, and the following solid state lasers: 488, 555, 633 nm located at the IDDRC facility, Boston Children's Hospital. Image analysis was performed using ImageJ (1.45S) and Metamorph Advanced Imaging Software. Immunofluorescence experiments in cell lines were performed three independent times. For experiments with W4 cells, images shown are representative of the population of cells that underwent cellular polarization. A fraction of polarized cells show weaker or stronger levels of cellular polarization; however, the images that are shown represent most of the polarized cell population.

**Immunohistochemistry.** $p53^{fl/fl}$, $p53/Lkb1^{fl/fl}$ mouse livers and $Kras^{G12D}$, $Kras^{G12D}/Lkb1^{fl/fl}$ mouse lungs were collected and fixed in neutral buffered formalin (4%; pH 7.0; 16–24 h, 20 °C), and then switched to 70% ethanol after 18–24 h. Tissues were embedded in paraffin and 5 µm sections were mounted on positively charged slides. Tissues were deparaffinized and antigen retrieval was performed in pH 6.0 citrate buffer for 30 min at 95 °C. ABC tissue staining was performed by using a modified protocol from Vector Laboratories VECTASTAIN Elite ABC kit (#PK-6101, #PK-2200). Briefly, the endogenous peroxidase was blocked by incubation in 0.3% hydrogen peroxide for 1 min. Sections were blocked in rabbit sera followed by primary antibody incubation overnight at 4 °C (YAP 1:100, Cell Signaling #4912; Scribble 1:400, Santa Cruz #1049; Ki67 1:50, DAKO MIB-5). Sections were washed and then incubated with HRP-conjugated secondary antibody (30 min; 20 °C), and developed with 3,3′-diaminobenzidine tetrahydrochloride (DAB)/$H_2O_2$. Counterstaining was done with haematoxylin and samples were washed, dehydrated, and mounted with Vectamount (Vector Labs #H-5000). Data obtained for immunohistochemistry analyses were repeated using sections from the same tissue and/or from amongst the same genotypic group. Representative images shown are from tissues that exhibit the least signal/noise background staining and represent most of the tissues that were analysed; however, there are some tissues that were stained that exhibited either more intense or weaker staining, which are not shown as they represented the minority of tissues examined.

**Immunoblotting.** Cell lines and tissues were collected, and processed for western blotting by solubilizing extracts in lysis buffer (50 mM Tris, 100 mM NaCl, protease inhibitor cocktail (Roche #04693159001) and phosSTOP (Roche, # 04906837001)). For standard immunodetection of proteins, 20 g of protein was used. For detection of phospho-proteins 30 g of total protein lysate was used. Protein lysates were then resolved by PAGE under reducing conditions (4–12% SDS–PAGE Bis-Tris gels; MOPS buffer system; Invitrogen; NuPAGE-MOPS system). The gels were blotted onto PVDF or nitrocellulose papers and blocked in either milk for standard antibodies or BSA for phospho-antibodies (phospho-antibodies blocked in PBS, 5% w/v BSA, 0.1% Tween-20 at dilutions: pYAP 1:1,000, Cell Signaling #4911; pMST1/2 1:1,000, Cell Signaling #3681; pLATS1/2 1:1,000, Cell Signaling #9153; pMARK 1:500, Cell Signaling #4836; pACC 1:1,000, Cell Signaling #3661; standard antibodies blocked in TBS-T, 5% w/v milk at dilutions: MST1 1:500, Cell Signaling #3682; Lats1 1:500, Cell Signaling #3477; MARK4 1:1,000 Cell Signaling #4834; LKB1 1:1,000 Santa Cruz sc-32245; Scribble 1:5,000, Santa Cruz sc-11049; MARK1 1:1,000 Cell Signaling #3319; AMPK 1:2,500, Cell Signaling #2603) for 1 h at room temperature, followed by incubation in primary antibodies diluted in blocking buffer. Unless otherwise stated, all primary antibody incubation steps were performed overnight at 4 °C. After washing in TBS-T, antigens were detected using HRP-conjugated secondary antibodies (1:20,000 in TBS-T: Thermo #32430, #32460, Santa Cruz #sc-2020), and visualized using enhanced chemoluminescence (Thermo, #34096). Immunoblots shown are representative of experiments that were repeated and reproduced at least three independent times. For some challenging experiments and antibodies, the representative blots are ones that show the least nonspecific background and have a low signal-to-noise ratio.

**Cell lines.** LS174T, HEK293T, DLD1, MCF7 and HaCaT cells were cultured in DMEM + 10% FBS in 5% $CO_2$, >95% humidity. A549 cells were cultured in RPMI-1640 supplemented with 2 mM L-glutamine and 10% FBS. The LS174T–W4 clone cell line was a gift from H. Clevers (Utrecht Institute, Netherlands). Other cell lines were acquired from the American Type Culture Collection (Manassas).

**Soft-agar colony-formation assay.** The base agar consisted of low-melting-point 0.6% agar dissolved in RPMI-1640 (Life Technologies, # 31800-022) or DMEM (Life Technologies # 12100046), 10% FBS and 1% penicillin/streptomycin. Base agar was allowed to set for at least 1 h before plating of the top agar. The top agar consisted of approximately 250 cells resuspended in 0.3% low-melting-point agar dissolved in RPMI or DMEM, 10% FBS, 1X penicillin/streptomycin in a well of a 6-well plate. Samples were incubated for 4 weeks following seeding and then stained with 0.1% crystal violet in 10% ethanol for 20 min. Wells were destained in distilled water 5 times or until the decanted water ran clear before imaging.

***In vitro* proliferation assay.** A colorimetric MTS assay (Promega, # G5430, Madison) was used to determine the proliferation rate for different cell lines. Experiments were done following the manufacturer's instructions. Briefly, 1,000 cells per well were cultured in triplicate into 96-well plates and incubated for 0–7 days. At the time of culture and each day for a total of 7 days, a plate was analysed by colorimetric reading (absorption of light at 450 nm).

**Mouse models.** Animal work was approved by the institutional committee at Boston Children's Hospital. Animals were housed in specific pathogen-free facilities at the hospital. The mouse models $p53^{flox/flox}$ (JAX Labs, B6.129P2-$Trp53^{tm1Brn}$/J), $LKB1^{flox/flox}$ (ref. 36), LSL-$KRAS^{G12D}$ (JAX Labs, 129S/Sv-$Kras^{tm4Tyj}$/J), $Yap1^{flox/flox}$ (ref. 11), PDX-Cre have been previously described[44]. For all experiments involving Ad-Cre-mediated deletion, female mice of approximately 5–6 weeks of age were used. Ad-Cre administration was performed between 2–4 weeks of age. Xenograft assays were performed in 5-week-old male Nu/J mice (JAX Labs, B6.Cg-$Foxn1^{nu}$/J), using $1 \times 10^6$ cells 100 $\mu l^{-1}$ volume of Matrigel (BD Biosciences). Metastasis assays were performed in 5-week-old male NOD/SCID mice (JAX Labs, NOD.CB17-$Prkdc^{scid}$/J) using $1 \times 10^6$ cells 100 $\mu l^{-1}$ volume of PBS injected intravenously. For induction in the liver, 100 µlof Ad-Cre was introduced intravenously at $1 \times 10^9$ pfu per mouse (Ad5CMVCre, University of Iowa, GTVC)[45]. No statistical method was used to predetermine sample size for treatment groups. There was also no requirement for animal randomization during the course of the animal studies.

**Tissue samples.** We studied formalin-fixed paraffin-embedded tissue-biopsy sections of diagnosed PJS and juvenile polyposis patients with confirmed mutations in LKB1, SMAD4 and PTEN respectively. Studies with patients' samples at Boston Children's Hospital were covered under IRB-CRM09-12-0660.

**Small-molecule inhibitors.** Metformin (10 mM) was from EMD Millipore, and AICAR (2 mM) and rapamycin (1 mM) were from TOCRIS Bioscience. MAP Kinase

Signaling Pathway Inhibitor Panel was purchased from EMD Millipore (#444189) and incubated according to the manufacturer's recommended concentrations (FR180204: $IC_{50} = 510$ nM, JNK II: $IC_{50} = 40$ nM for JNK-1 and JNK-2 and 90 nM for JNK-3, JNK IX: $pIC_{50} = 6.5$, MEK1/2: $IC_{50} = 220$ nM, MK2a: $IC_{50} = 60$ nM, Inhibitor 5: $IC_{50} = 40$ nM, PD98059: $IC_{50} = 10\,\mu$M, Inhibitor IV: $IC_{50} = 10$ nM, SB203580: $IC_{50} = 600$ nM, TPL2 Inhibitor: $IC_{50} = 50$ nM, ZM336372: $IC_{50} = 70$ nM).

**Luciferase assays.** For stable cell lines expressing STBS–luciferase, cell lysates were analysed using Dual-glo luciferase assay (Promega, #E2940). Alternatively, cell lines not containing the reporter were transiently transfected with the STBS-firefly-luciferase and firefly-*Renilla* constructs using Lipofectamine 2000 (Life Technologies) and assayed 48 h following plasmid transfection (Berthold Technologies).

**Microarray and gene set enrichment analysis.** Reverse transfection of RNAi oligonucleotides for NF2, LATS2, YAP, TAZ and Scrambled RNAi was performed in HEK293T, HaCaT and DLD1 cells with RNAiMAX (Invitrogen) according to the manufacturer's instructions. Duplicate samples were prepared for each condition. Four days after transfection, confluent cell culture was collected for RNA extraction with the Trizol reagent (Invitrogen). RNA quality assessment, cDNA synthesis, probe generation, array hybridization and scanning were carried out by Boston Children's Hospital Molecular Genetics Microarray Core Facility. Data sets were analysed with the online microarray analysis software GenePattern (Broad Institute) with default settings. Differentially expressed genes were defined as those with at least a twofold change in NF2/LATS2 double-knockdown cells and a $P$ value smaller than 0.05. To generate a generic Hippo target gene signature, genes upregulated in all three NF2/LATS2 double-knockdown cell lines were combined, and those without a gene symbol were eliminated from the list. For gene set enrichment analysis, we used a data set from published gene expression profiles of lung adenocarcinomas developed in $Kras^{G12D}$, $Kras^{G12D}Lkb1^{f/-}$ or $Kras^{G12D}Lkb1^{f/f}$ mouse models[36]. The enrichment analysis was performed in the GSEA software available from the Broad Institute with the default settings.

**Microarray accession numbers.** Microarray data generated for this study have been deposited in the GEO database under accession number GSE49384. The published microarray data set[36] re-analysed in this study is available from the GEO database under accession number GSE6135.

**Statistical analyses.** No statistical method was used to predetermine sample size. For experiments using LS174T-W4 cells, we always included a $-/+$ Dox control to detect the level of activity of LKB1 in inducing cell polarity. Experiments were discarded in which Dox administration had less than 50% affect on cell polarization. For biochemical experiments, we performed experiments at least three independent times to be confident in the experimental reproducibility. In some cases, experiments were repeated more than 3 times to ensure validity of our hypotheses. Investigators were not blinded to allocation during experiments and outcome assessment. All statistical analyses were performed by SAS program (Version 9.1, SAS Institute). All $P$ values were two-sided and statistical significance was set at $P = 0.05$. For categorical data, the $\chi^2$ test was performed. For the experiments shown, the variance was similar between groups that were being statistically compared.

44. Morton, JP *et al*. LKB1 haploinsufficiency cooperates with Kras to promote pancreatic cancer through suppression of p21-dependent growth arrest. *Gastroenterology* **139,** 586–597 (2010).
45. Stec, D. E., Davisson, R. L., Ha skell, R. E., Davidson, B. L. & Sigmund, CD. Efficient liver-specific deletion of a floxed human angiotensinogen transgene by adenoviral delivery of CRE-Recombinase *in vivo*. *J. Biol. Chem.* **274,** 21285–21290 (1999).

# CORRIGENDUM

## A genetic screen identies an LKB1–MARK signalling axis controlling the Hippo–YAP pathway

**Morvarid Mohseni, Jianlong Sun, Allison Lau, Stephen Curtis, Jeffrey Goldsmith, Victor L. Fox, Chongjuan Wei, Marsha Frazier, Owen Samson, Kwok-Kin Wong, Carla Kim and Fernando D. Camargo**

*Nat. Cell Biol.* **16,** 108–117 (2014); published online 22 December 2013; corrected after print 7 January 2014

In the version of this Article originally published, the name 'Kwok-Kin Wong' was spelled incorrectly in the author list. This has now been corrected in all online versions of the Article.

DOI: 10.1038/ncb2884

nature cell biology

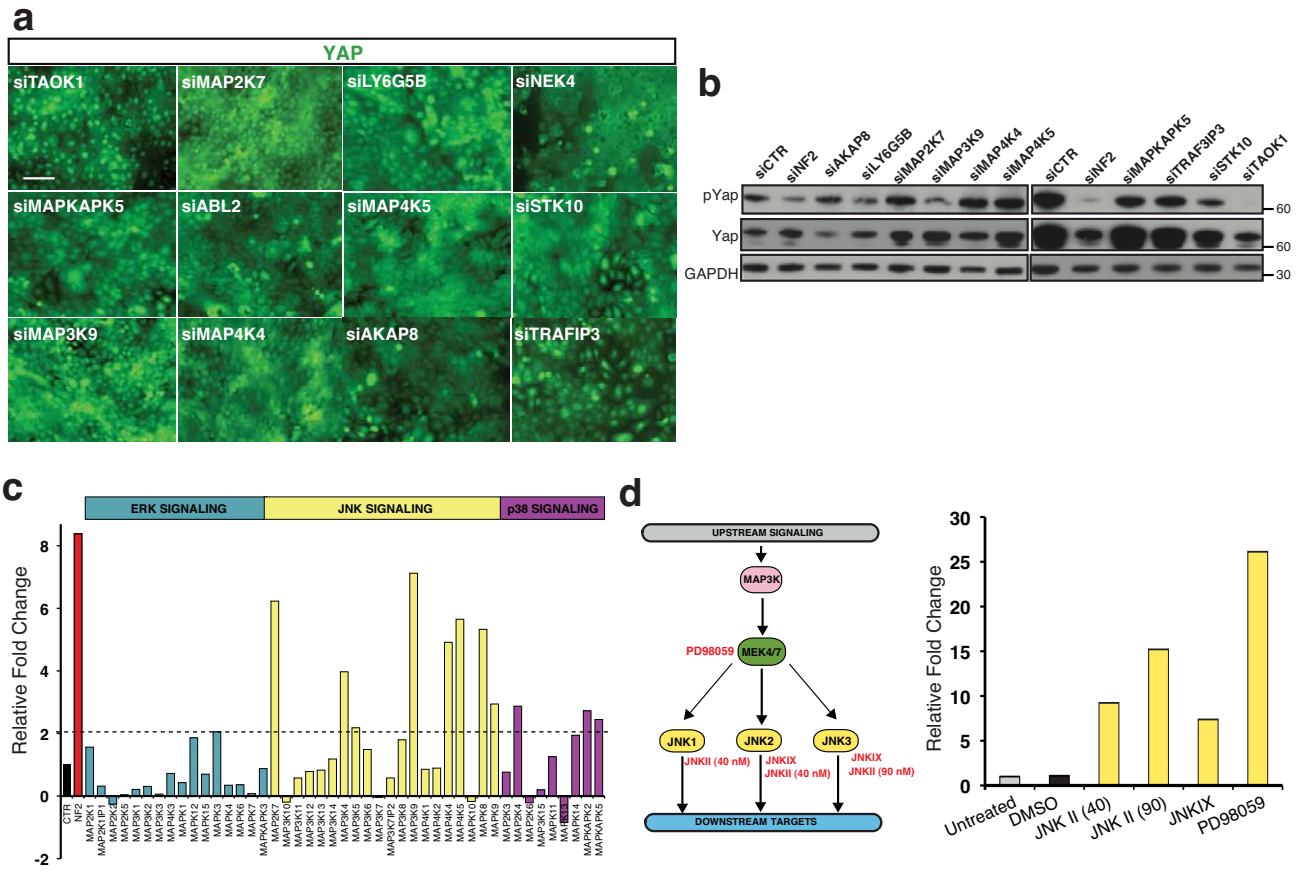


**Supplementary Figure 1** Identification of kinases that can modulate the Hippo Signaling Pathway *in vitro*. (a) Immunofluorescence for YAP localization in confluent HaCaT cells following siRNA transfection of selected kinase hits. Scale bars, 200μm. Experiment was repeated 3 times independently (b) Western Blot for YAP S127 phosphorylation, and total YAP in 293T cells four days following siRNA transfection of selected kinase hits. Representative blot is shown. This experiment was repeated 3 independent times (c) Mitogen activated kinase pathway siRNA mini-screen using the STBS-luciferase reporter in 293T cells compared to scrambled control (CTR). Data shown is from technical triplicates. The experiment was repeated in three independent experiments. 5 bD) Selective JNK small molecule screen using the STBS-luciferase reporter in 293T cells. Schematic demonstrates where the inhibitors function. Fold changes calculated are compared to untreated controls.

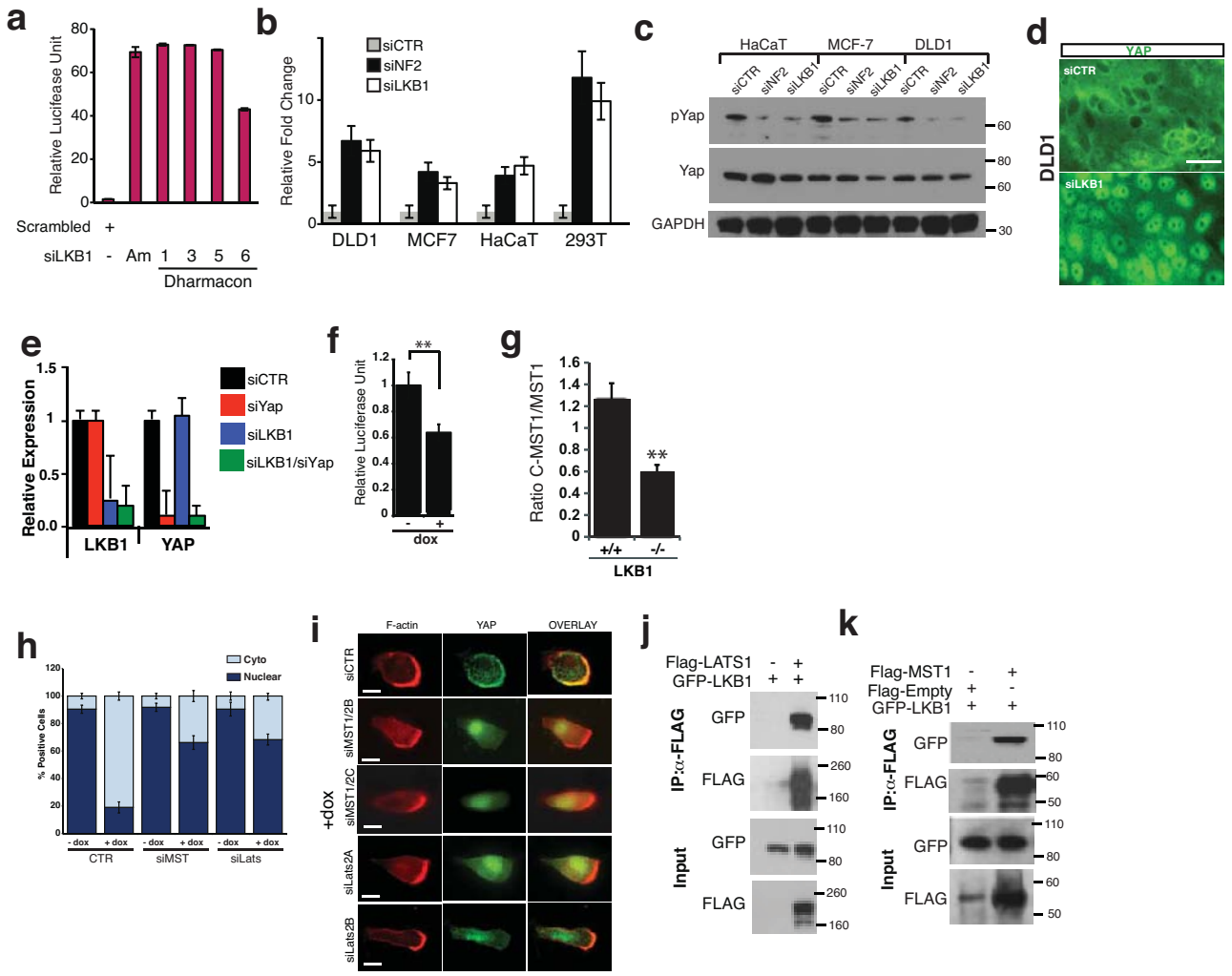


**Supplementary Figure 2** LKB1 acts upstream of the Hippo Signaling Pathway in vitro and *in vivo*. (a) Knockdown of LKB1 using multiple different siRNA oligos increases STBS-luciferase reporter activity in 293T cells. n= 5 biological replicates ± SD. (b) Knockdown of LKB1 reproducibly increases STBS-luciferase reporter activity across various cell lines. n=3 biological replicates. Error bars represent mean ± SD. (c) Knockdown of LKB1 reproducibly decreases YAP S127 phosphorylation across various cell lines by western blot analysis. (d) Knockdown of LKB1 in DLD1 cells promotes YAP nuclear localization at confluent cell densities. Experiment has been performed independently three times. Scale bar, 200μm (e) qPCR validation of LKB1 and YAP siRNA knockdown in 293T cells. n=3 biological replicates, ± SD. (f) LKB1 activation in W4 cells repressed TEAD-reporter activation. n= 3 replicates per biological triplicate (g) Decreased activity of MST1/2 in LKB1 deficient livers. Ratio of cleaved MST1 versus full length MST is shown for an average from n=4 mice. (h) Quantification of YAP localization in W4 cells following MST1/2 or LATS1/2 knockdown. Data are derived from three independent experiments where at least 300 cells where scored. N = 3, error bars represent mean ± SD. (i) Validation of MST1/2 and LATS2 downstream of LKB1 using two additional sets of siRNAS. Representative figure from three independent experiments is shown. Scale bars, 20μm (j, k) Immunoprecipitation of overexpressed LKB1, LATS1, and MST1 in 293T cells. Representative blot is shown. Experiment has been performed three times independently. Error bars represent mean ± SD from triplicate samples. **, P≤ 0.01, two-tailed t-test.

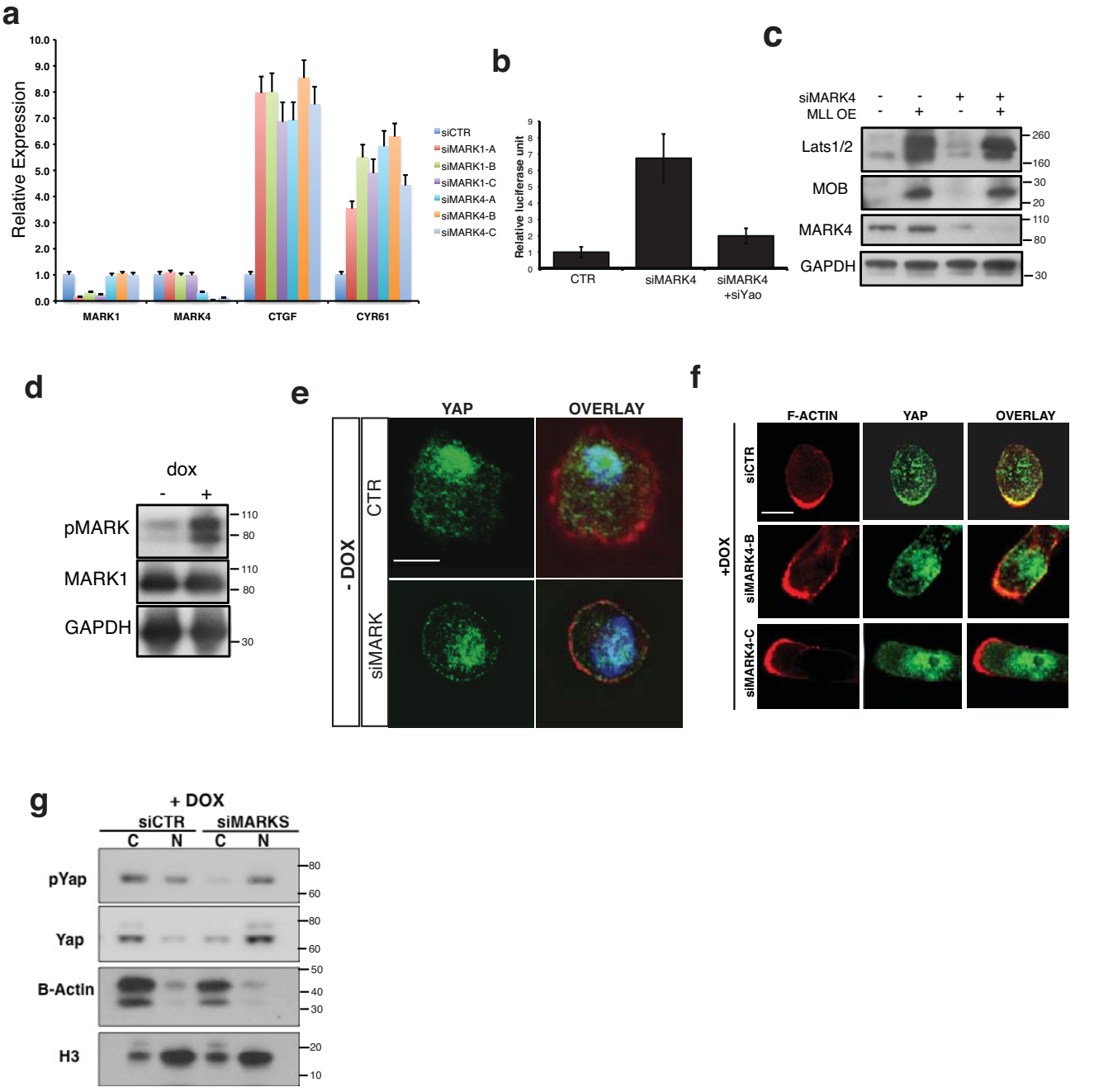


**Supplementary Figure 3** Yap1 activity and localization is dependent on the LKB1 substrate, MARKs. (a) qPCR validation of siRNA knockdown of MARK1 and MARK4 and expression of YAP-target genes, CTGF and CYR61. n=3 biological replicates (b) STBS reporter activity following knockdown of MARK4 and YAP in 293T cells. n=3 biological replicates (c) Western blot showing expression level of Mob1/LATS1/LATS2 in MARK4 knockdown cells. Representative blot is shown from three independent experiments (d) Activation of LKB1 in W4 cells promotes activation of MARKs as measured by Thr215 phosphorylation (MARK1) in the kinase activation loop. Representative blot is shown from three independent experiments (e) Immunofluorescence for YAP localization (green) and cell polarization (red) in doxycycline-untreated W4 cells following knockdown of MARK4. N= 3 biological replicates. Each experiment was performed with technical triplicates. Scale bar, 20μm. (f) YAP localization in W4 cells following LKB1 activation and knockdown of MARK4 using 2 independent siRNA's. Three independent experiments were performed. Scale bars, 20μm. (g) Biochemical analysis of phospho-YAP localization by subcellular fractionation of W4 cells treated with doxycycline and MARK knockdown. Representative blot from three independent experiments is shown. Error bars represent mean ± SD.

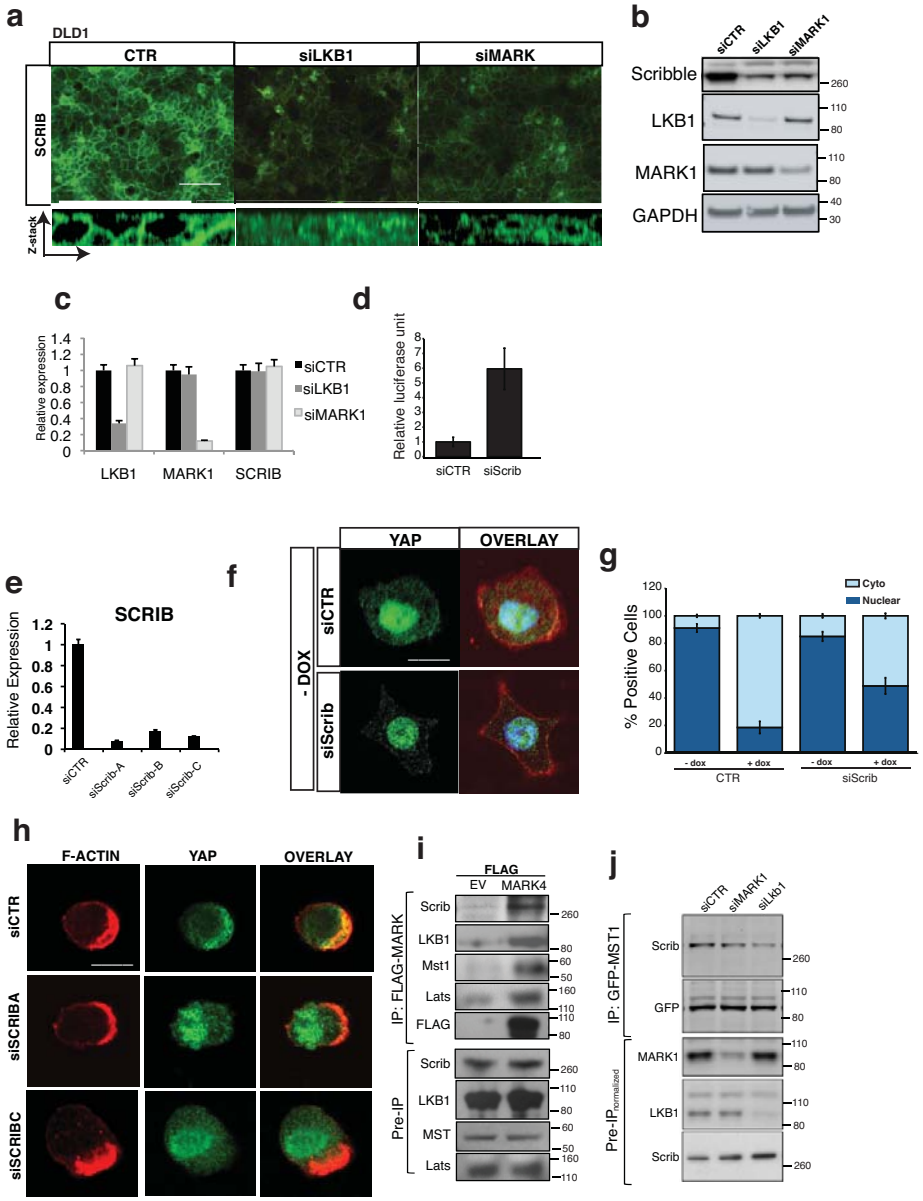


**Supplementary Figure 4** Scribble expression and correct localization is required for Yap1 activity. (a) Immunofluorescence for Scribble (SCRIB) localization (green) in DLD1 cells following LKB1 and MARK siRNA knockdown. Experiment was repeated three times. Scale bar, 200μm. (b-c) Immunoblot and qPCR for SCRIB expression following LKB1 and MARK1 knockdown in MCF7 cells. n=3 biological triplicates (d) siRNA knockdown of SCRIB in 293T cells induces TEAD-reporter activity. n = 3 independent experiments. (e) qPCR validation of SCRIB knockdown using 3 independent siRNA's. n= 3 independent experiments. (f) Immunofluorescence for YAP localization (green) and cell polarization (red) in doxycycline-untreated W4 cells following knockdown of SCRIB. Biological replicates were performed three times. Scale bar, 20μm. (g) Quantification of YAP localization in W4 cells following scribble knockdown. Data are derived from three independent experiments where at least 300 cells where scored. (h) Immunofluorescence for YAP localization following activation of LKB1 and knockdown of scribble using 2 independent siRNA's. Scale bar 20μm. (i) Immunoprecipitation of overexpressed MARK4 with SCRIB, LKB1, MST1, and LATS1. Experiment was repeated three times. (j) Immunoprecipitated SCRIB in MARK1-knockdown cells show decreased interaction with MST and LATS. Experiment was repeated three times. Error bars represent mean ± SD.

**a** **Hippo Signature**

| | | | |
|---|---|---|---|
| ABL2 | MID1 | FST | SLC16A6 |
| ACAT2 | MIR622 | GADD45A | SLC2A3 |
| ACLY | MYBL1 | GADD45B | |
| ACSL1 | MYOF | GCNT4 | SLC43A3 |
| ACSL4 | NCF2 | GDPD3 | SLC48A1 |
| ACSS2 | NFKBIA | GGT5 | SLC5A1 |
| ADAMTS12 | NID2 | GPCPD1 | SLC5A3 |
| AMOTL2 | NPPB | GPRC5A | SLC7A7 |
| ANKRD1 | NT5DC3 | GPRC5B | SLCO2A1 |
| ANXA3 | NT5E | HBEGF | SLIT2 |
| AREG | NUAK2 | HMGCS1 | SNAPC1 |
| AXL | OLFML3 | HSPB8 | SNORA75 |
| BCAS1 | OLR1 | HSPC159 | SNORD13P2 |
| C6ORF155 | OPN3 | ICAM1 | SNORD21 |
| CALB2 | P2RY8 | IDI1 | SNORD38A |
| CCL28 | PCYT2 | IFFO2 | SNORD53 |
| CCL5 | PDCD1LG2 | IFIT2 | SNRPG |
| CD55 | PDP2 | IGFL1 | SQLE |
| CDH2 | PHLDA1 | IL1A | STXBP1 |
| CHST9 | PLAU | IL1B | SYT14 |
| CLDN1 | PLAUR | IL32 | TFPI2 |
| CLDN4 | PLK2 | IL8 | TGFA |
| CLMN | PLK3 | INSIG1 | TGFB2 |
| COTL1 | PRRG1 | ITGA5 | TGM2 |
| COX6C | PSAT1 | ITGBL1 | THBS1 |
| CPA4 | PSG5 | JPH1 | TIMP2 |
| CRYAB | PTPN14 | KLK7 | TLCD1 |
| CTGF | RAB11FIP1 | KPNA7 | TMEM154 |
| CTH | RAB3B | KRT18 | TMEM171 |
| CTNNAL1 | RBM14 | | TMEM27 |
| CYR61 | RBMS2 | KRT8 | TNF |
| CYTH3 | RGNEF | KRT81 | TNFAIP3 |
| DENND3 | RIMKLB | LAMB1 | TNFRSF9 |
| DHCR7 | RND3 | LDLR | TNFSF18 |
| EBP | SAA1 | LIF | TSC22D2 |
| ENC1 | SAA2 | LIPH | TUFT1 |
| EPB41L2 | SC4MOL | LMBRD2 | UBD |
| ERRFI1 | SCD | LOC100130876 | UCA1 |
| EXPH5 | SCD5 | LOC642947 | UCP2 |
| F3 | SCML1 | LOXL4 | UGCG |
| FASN | SEMA7A | LPHN2 | UPK1B |
| FDFT1 | SERPINB10 | LPIN1 | UPP1 |
| FDPS | SERPINB2 | MACC1 | VGLL1 |
| FGFBP1 | SHROOM3 | MFAP5 | WIPI1 |
| FLNA | SLC16A13 | MICB | |

**b**

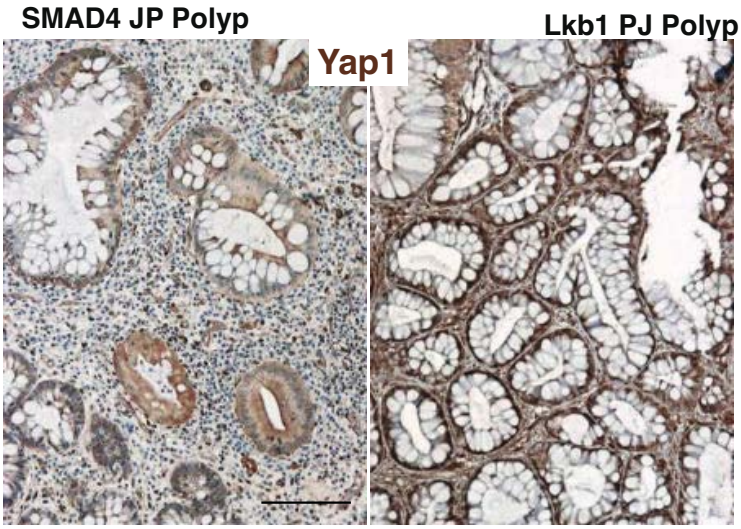


**Supplementary Figure 5** Generation of a Hippo Gene Expression Signature and localization of Yap in human LKB1-mutant tissues. (a) Microarray analysis on three different cancer cell lines reveal a core set of genes whose expression changes following siRNA knockdown of NF2 + LATS1/2, and for which this response is dependent on YAP/TAZ. Differentially expressed genes were defined as those with at least 2 fold change in NF2/LATS2 double knockdown cells and a p value smaller than 0.05. (b) YAP immunohistochemistry on human SMAD4 juvenille polyposis (JP) intestinal polyp compared to a human LKB1 mutant Peutz-Jeghers (PJ) intestinal polyp. Scale bar, 500 μm.

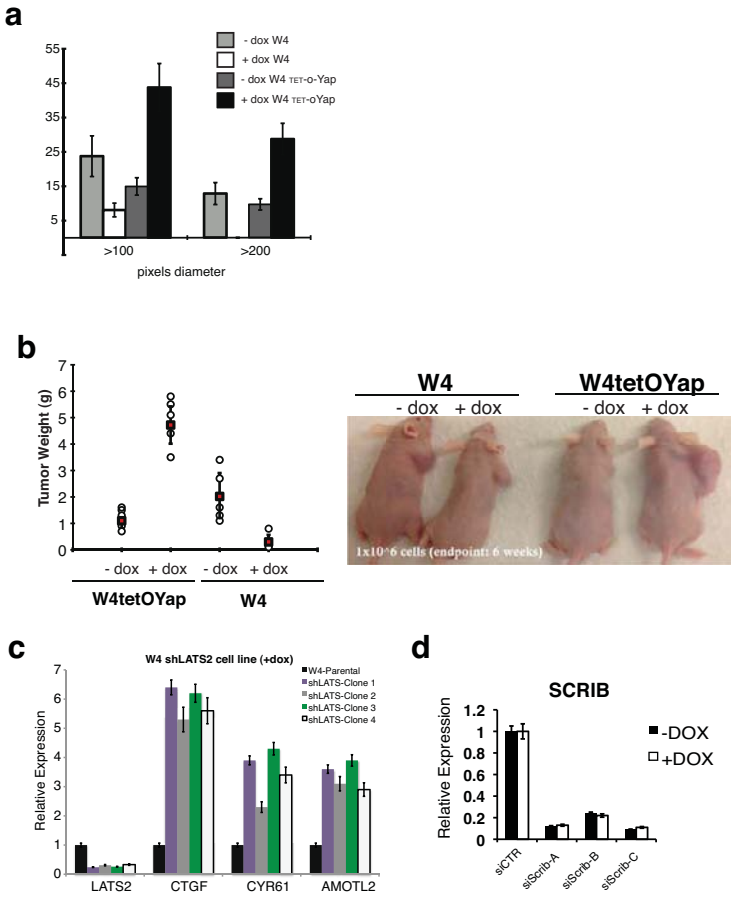


**Supplementary Figure 6** Yap1 acts downstream of LKB1 and can overcome LKB1 tumor suppressive function. (a) Quantification of triplicate samples of number and size of W4, W4TetOYAP, +/- doxycycline colonies in soft agar assays. n= 3 biological triplicates (b) Tumor weights of W4, W4TetOYAP, +/- doxycycline after seven weeks. Representative images of nude mice carrying xenografts with W4, W4TetOYAP tumors. N = 7 mice per each of the four genotypes. (c) qPCR validation of shRNA knockdown of LATS2 and activation of YAP-target genes in W4 cells. N = 3 biological replicates. (d) qPCR of Scribble following Scribble siRNA knockdown in the presence of LKB1 activation. n= 3 biological replicates. Error bars represent mean ± SD.

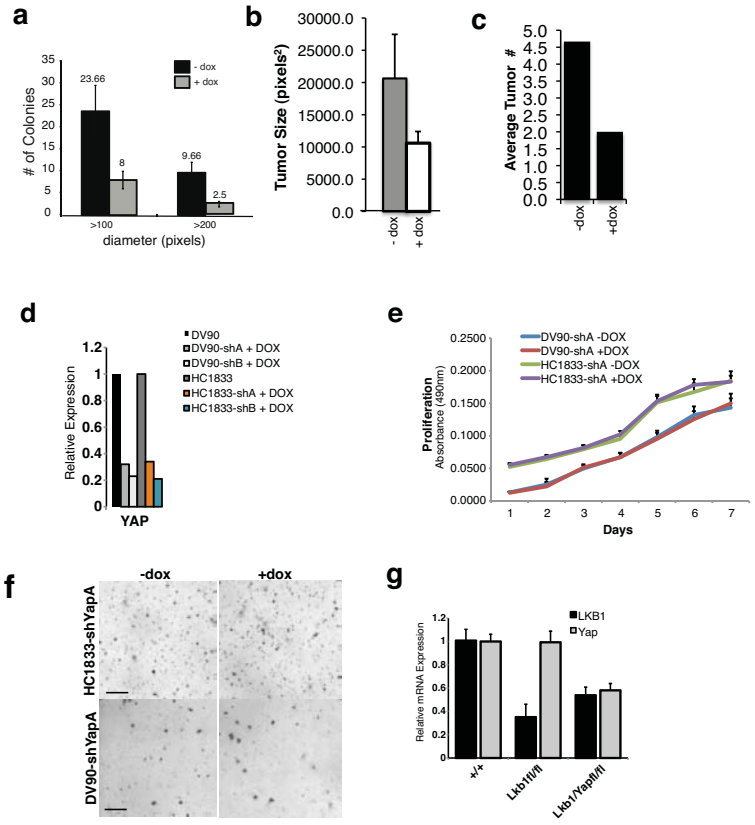


**Supplementary Figure 7** Loss of Yap1 in LKB1 mutant xenograft show tumor growth inhibition. (a) Quantification of triplicate samples of number and size of W4, W4TetOYAP, +/- doxycycline colonies. n=3 biological replicates (b-c) Average tumor size and number per mouse following intravenous injection of $1x10^6$ A549iYAPshRNA cells (-/+ doxycycline) for 6 weeks. n=3 mice per group (d-f) Two cell lines that are low in YAP target gene expression were infected with shYAP1 hairpins and assessed for proliferation using MTS assays (e) and soft agar colony formation assay (f) n = 3 biological replicates. Scale bar, 500 μm. (g) Expression levels of LKB1 and YAP following Ad-cre administration in Lkb1-floxed and Lkb1/YAP floxed livers. n= 4 mice per genotype. Error bars represent mean ± SD.

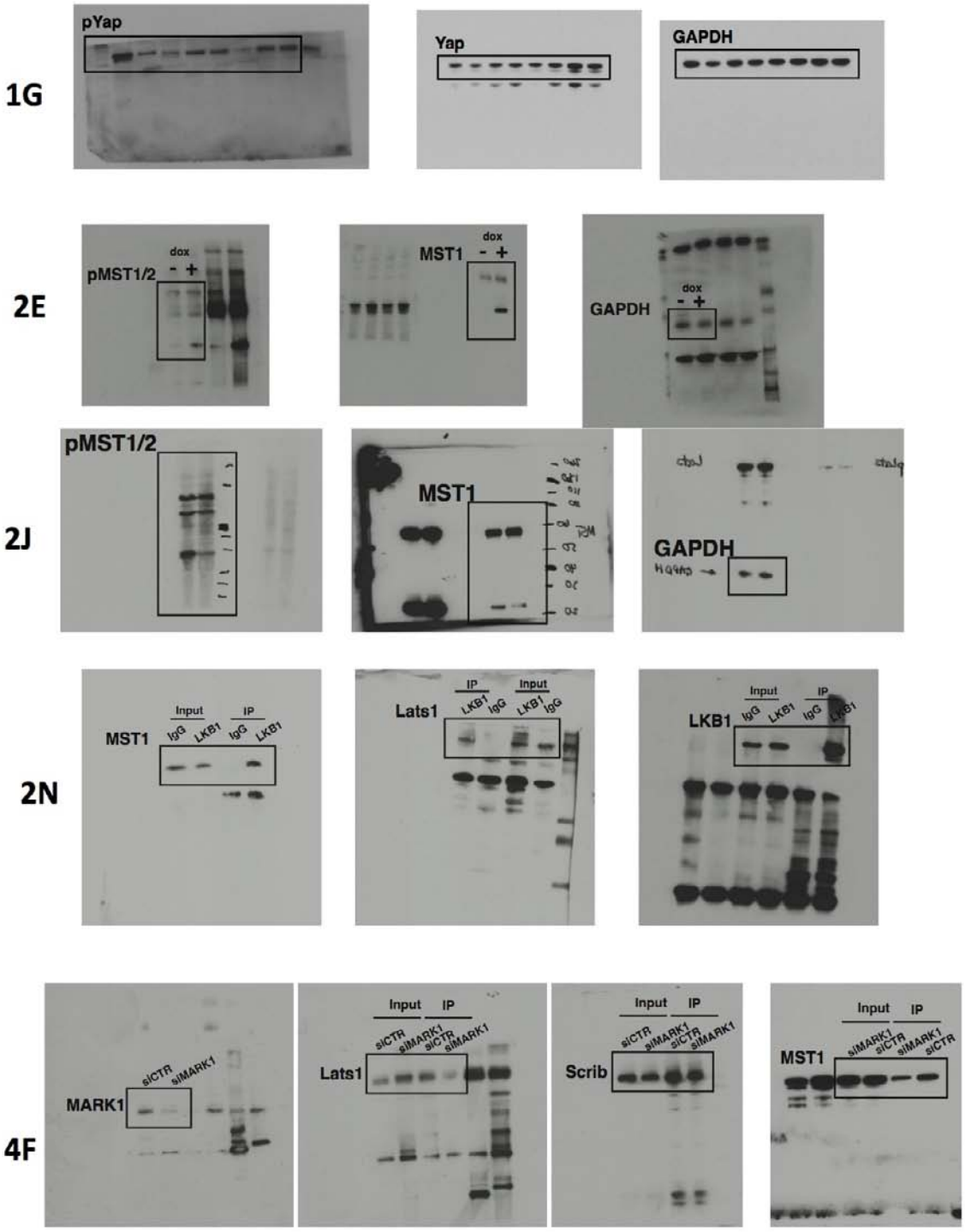


**Supplementary Figure 8** Full scans